THE ASTRONOMICAL JOURNAL, 119:1881–1900, 2000 April

PROFILES OF STRONG PERMITTED LINES IN CLASSICAL T TAURI STARS[1]

SILVIA H. P. ALENCAR[2,3] AND GIBOR BASRI[2]
Received 1999 September 26; accepted 2000 January 4

ABSTRACT

We present a spectral analysis of 30 T Tauri stars observed with the Hamilton echelle spectrograph over more than a decade. One goal is to test magnetospheric accretion model predictions. Observational evidence previously published supporting the model, such as emission-line asymmetry and a high frequency of redshifted absorption components, are considered. We also discuss the relation between different line-forming regions and search for good accretion rate indicators. In this work we confirm several important points of the models, such as the correlation between accretion and outflow, broad emission components that are mostly central or slightly blueshifted, and only the occasional presence of redshifted absorption. We also show, however, that the broad emission components supposedly formed in the magnetospheric accretion flow only partially support the models. Unlike the predictions, they are sometimes redshifted and are mostly found to be symmetric. The published theoretical profiles do not have a strong resemblance to our observed ones. We emphasize the need for accretion models to include a strong turbulent component before their profiles will match the observations. The effects of rotation, as well as the outflow components, will also be needed to complete the picture.

Key words: stars: formation — stars: pre–main-sequence

1. INTRODUCTION

Classical T Tauri stars (CTTSs) are young, almost solar-mass stars that exhibit a wide range of permitted and sometimes also forbidden emission lines, together with an excess continuum emission that goes from the infrared to the ultraviolet. Their spectral energy distribution is consistent with the presence of a circumstellar disk that appears to play a major role in the regulation of both the infall and outflow of material from the star-disk system. A strong wind component is also thought to be present and to cause the blueshifted absorption features commonly seen in the Balmer lines.

In the past years many attempts have been made to explain those characteristics. The permitted line emissions were discussed in terms of outflowing winds (Hartmann, Edwards, & Avrett 1982; Hartmann et al. 1990; Natta & Giovanardi 1990), turbulence in a boundary layer between the disk and the stellar surface (Bertout, Basri, & Bouvier 1988; Basri & Bertout 1989), and chromospheric activity (Calvet, Basri, & Kuhi 1984; Calvet et al. 1985). More recently, magnetospheric accretion models were proposed (Hartmann, Hewett, & Calvet 1994; Shu et al. 1994; Hartmann 1998). In these models the circumstellar disk is truncated by stellar magnetic field lines and the strong broad emissions arise from the accelerated infalling material channeled through the lines that connect the disk to the star. At the base of the magnetospheric accretion column, where the accreted material hits the star, hot spots and the hot continuum emission (veiling) are produced.

Edwards et al. (1994) showed observational evidence in a sample of 15 CTTSs that they claimed confirm some of the magnetospheric predictions, such as blueward asymmetric emission lines (due to disk occultation of the receding flow) and redshifted absorption components at typical free-fall velocities (inverse P Cygni profiles), which are naturally explained by the magnetospheric infall. The line profiles of several stars were also well reproduced by magnetospheric calculations (Muzerolle, Hartmann, & Calvet 1998a; Najita, Carr, & Tokunaga 1996), but often the theoretical profiles are more asymmetric and always less broadened than the observed ones. However, we must keep in mind that the models of Hartmann et al. (1994) do not include rotation and winds that would certainly influence both the asymmetry and the broadening of the theoretical profiles.

The CTTSs were initially found to be slow rotators, based on observational surveys that reported a bimodal distribution of stellar rotation periods among TTSs (Choi & Herbst 1996), where the slow rotators ($P > 4$ days) seemed to exhibit disk signatures, as near-infrared excess emission, that the fast rotators did not (Edwards et al. 1993). It has always been a challenge to understand the spin-down of those stars, but the magnetospheric model predicts that the magnetic interaction between the star and the disk could regulate the stellar rotation. This could explain why weak T Tauri stars (WTTSs), that do not have disks present a wider range of rotational periods. Recently, Stassun et al. (1999), analyzing the rotation period distribution of young stars in the Orion nebula region, showed that this bimodal distribution does not seem to exist and that the conclusion of the earlier work was also statistically consistent with a uniform distribution. Herbst, Rhode, & Hillenbrand (1999) suggest this recent result, however, may be confined to low-mass TTSs.

In view of the many points still under discussion, we present in this paper the spectral analysis of an observed sample of 30 TTSs with a large spectral coverage, which are used to analyze the magnetospheric model's predictions and test the previous observational results. The observations and reduction procedures are described in § 2, and the equivalent width and veiling measurements are detailed in § 3. We analyze the many features in our spectra in § 4,

[1] Based on observations obtained at Lick Observatory.

[2] Department of Astronomy, University of California at Berkeley, Berkeley, CA 94720-3411; silvia@crater.berkeley.edu, basri@soleil.berkeley.edu.

[3] Departamento de Física, Instituto de Ciências Exatas, Universidade Federal de Minas Gerais, C.P. 702, 30123-970, Belo Horizonte, MG, Brazil.

discuss the results in § 5, and draw our final conclusions in § 6.

2. OBSERVATIONS

We present the spectral analysis of a sample of 30 TTSs listed in Table 1. The observations, which span over more than a decade, were carried out at Lick Observatory with the 3 m Shane Telescope and the Hamilton echelle spectrograph (Vogt 1987) coupled either to a TI 800 × 800 CCD or a Ford 2048 × 2048 CCD. With the smaller detector, two settings were established: a red setting covering 52 orders from 4900 up to 8900 Å and a blue setting covering 38 orders from 3900 up to 5200 Å. The spectral coverage, however, is not complete, with a gap of a few dozens of angstroms between orders. Whenever possible, blue and red observations were obtained in the same night or within one night of difference, but for some stars we only have the red setting. The bigger CCD installed in 1992 permits a full spectral coverage of approximately 92 orders ranging from 3900 to 8900 Å. The mean resolution of the spectrograph is $\lambda/\Delta\lambda \approx 48{,}000$ and the exposure times varied from 15 minutes to 1 hr 15 minutes, depending on the target and on the CCD used.

The reduction was performed in a standard way described by Valenti (1994), which includes flat fielding with an incandescent lamp exposure, background subtraction, and removal of cosmic rays. Wavelength calibration is made by observing a thorium-argon comparison lamp and performing a two-dimensional solution to the thorium lines. Radial and barycentric velocity corrections are applied and all the data shown are in the stellar rest frame. The spectra are not flux calibrated, so each spectrum has been continuum normalized. Due to differences in weather conditions, exposure times, and efficiency between different chips, there is a wide range of signal to noise in the data. However, not only strong emission-line profiles were reliably extracted, but also many absorption-line profiles as shown in Figure 1. After the reduction procedure the spectra have been binned and smoothed with a window width of 3. A weak-line T Tauri star was included in the sample (V410) (Tau Herbig & Bell 1988), as a reference to stars without disk accretion. DQ Tau is a known binary system (Basri, Johns-Krull, &

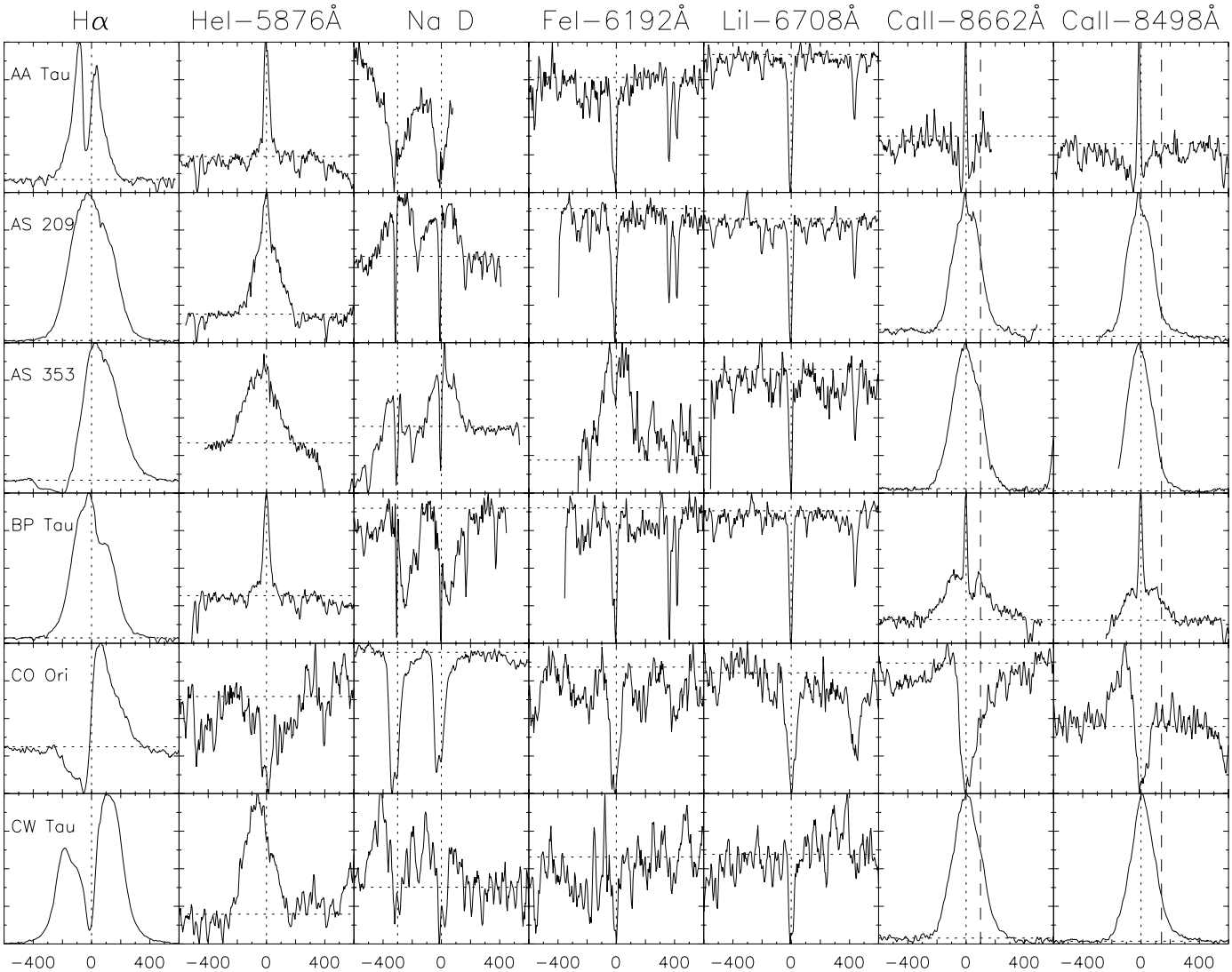

FIG. 1.—Line profiles. All data have been continuum normalized, binned, and smoothed with a window width of 3. The horizontal dotted lines represent the continuum level at 1. The vertical dotted lines are the spectral line's center at the stellar rest frame. The contamination of the Na D lines by the vapor lamps of the city of San Jose has been removed. The dashed lines close to the IRT profiles are the velocity position of the blended Paschen emission lines. The *x*-axes are radial velocities in km s^{-1} and the *y*-axes correspond to relative intensities.

TABLE 1

LINE EQUIVALENT WIDTHS (Å) AND VEILINGS

STAR	UT DATE Red/Blue	Hα	Hβ	Hγ	Hδ	He I	NaD1+D2	Fe I λ6192	Li I λ6708	Ca II λ8662	Ca II λ8498	Ca K	Fe I λ5497	Fe II λ4924	Fe II λ4352	VEILING red	VEILING blue
AA Tau.....	1989 Oct 13/13	14.2	2.2:	3.5:	2.7	1.2	−4:	−0.3	−0.6	0.5	0.7	2.2	−0.3	x	x	0.3	0.2
AS 205.....	1987 Jun 10/	111.1				1.6	2.5	−0.2	−0.1	20.4	39.7		−0.1			0.2	
AS 209.....	1987 Oct 6/6	113.4	33.5	11.5	7.9	3.3	2.9	−0.3	−0.4	16.6	21.0	21.6	−0.2	x	x	0.3	0.3
AS 353.....	1987 Sep 6/6	56.0	12.6	5.9:	−2.9	2.6	2.9	0.7	−0.1	37.9	36:	x	0.0	5.6	3.8	1.7	2.4
BP Tau	1986 Dec 21/21	48.6	10.7	4.5	4.8	1.0	−1.1	−0.2	−0.4	4.1	3.5	11.6	−0.2	x	x	0.5	0.9
CI Tau.....	1987 Oct 12/	110.1				3.4	−0.5	−0.3	−0.4	19.7	19:		−0.2	3:		0.2	
CO Ori	1992 Nov 15	2.9	−2.2	−3:	−2.9	−0.1:	−2.2	−0.2	−0.2	x	0.2	x	−0.2	x	x	0.2	0.2
CW Tau	1998 Nov 3	109.6	12.3	x	x	1.9	x	−0.1	−0.1	21.5	28.3	3:	x	2.2	x	1.5	x
DE Tau	1988 Feb 4/4	66.5	44.0	34.6	x	2.6:	x	x	−0.4	7.1	7.9	76.4	x	x	1.7	x	x
DF Tau	1992 Nov 14	61.0	6.8	3.0	3.2	3.0	0.8	x	−0.2	4.9	5.3	7.5	x	0.8:	0.1:	1.8	1.8
DG Tau	1993 Oct 30	60.5	17.7	8.2	5.4	2.4	2.5	0.3	−0.2	41.4	44.2	20.8	−0.1	5.0	3.0	2:	2:
DK Tau	1987 Oct 12/12	16.7	4.4	0.9	2.1	1.0	−2.1	−0.2	−0.4	2.1	2.7	3.5	−0.2	x	x	0.4	0.7
DL Tau	1998 Nov 3	110.2	24.8	7.2	3.4	5.4	7.0	−0.1	−0.2	39.9	46.5	8.5	x	7.3	x	1.9	x
DN Tau	1986 Nov 12/12	15.7	5.6	1.9	3.9	0.3	−3.4	−0.3	−0.6	0.4	0.5	10.6	−0.3	x	x	0.1	0.2
DO Tau	1998 Nov 3	58.2	5.3	x	x	2.1	2.4	x	−0.2	8.8	7.9	0.9:	x	1.9	x	0.9	x
DQ Tau	1993 Dec 24	157.1	23.4	3.3	2:	2.7	1.8	−0.1	−0.3	2.7	2.3	x	x	2.0	x	1.5	1.5
DR Tau	1998 Nov 3	81.0	5.3	1.0	1.5	4.2	4.0	x	−0.1	23.3	25.4	11.2	x	2.4	0.7	2.5	x
DS Tau.....	1987 Oct 11/11	27.3	7.2	4.6	3.7	0.9	−0.5:	−0.2	−0.2	0.4	0.3	19.9	−0.1	x	x	0.6	0.5
GG Tau	1989 Jan 17/18	40.2	8:	4:	2:	0.8	−2:	−0.2	−0.5	2.3	2.4	x	−0.2	x	x	0.3	1.1
GK Tau	1988 Feb 4/4	34.0	9.6	6:		1:	x	x	−0.6	4:	1.1	6.9	−0.3	x	x	x	0.1
GM Aur....	1987 Oct 11/11	63.5	12.4	4:	4.8	0.7	−2.1	−0.3	−0.4	0.3	0.4	32.5	−0.3	x	x	0.2	0.1
GW Ori	1993 Dec 23	31.5	2.9	x	x	x	1.4	−0.2	−0.2	4.7	5.2	x	−0.1	x	x	0.2	x
HL Tau	1986 Nov 12/	34.7				1.2	3.8	−0.2:	−0.2	28.2	30.6		x	2.5:		0.9	
RW Aur	1986 Dec 21/21	45.9	4.1	−2.1	−1.2	0.6:	−8.3	0.6	−0.2	27.5	37:	14.0	x	x	x	2.0	2.9
RY Tau.....	1986 Dec 21/21	12.4	−1.4:	−0.8:	−0.9	−0.3	0.2	−0.2:	−0.2	4.7	5.2	2.2	−0.2	x	x	0.1	0.0
SU Aur	1986 Nov 14/14	6.1	−1.7	−1.1:	−1.6:	−0.3	−1.0	−0.2	−0.2	−1.0	−0.7:	x	−0.3	x	x	0.0	0.0
T Tau	1989 Oct 13/13	63.1	9.8	3:	3.3	0.5	0.7:	−0.2	−0.4	11.2	13.7	27.7	−0.2	1.4:	x	0.1	0.1
UX Tau	1986 Dec 22/	3.5				x	−2.0	−0.3	−0.4	0.2	0.2		−0.3			0.0	
UY Aur	1988 Feb 4/4	97.0	20.8	10.7		2.6	x	x	−0.4	7.8	12:	96.2	x	x	x	0.1	0.8
V410 Tau...	1992 Nov 14	2.9	x	x	x	x	−3.4	−0.3	−0.5	0.2	0.2	2.2	−0.3:	x	−1:	0.1	0.2

NOTE.—When the lines could not be reliably used, the equivalent width and veiling were not measured (marked with an "x") and when we did not have a spectrum at a given wavelength the cell is left blank.

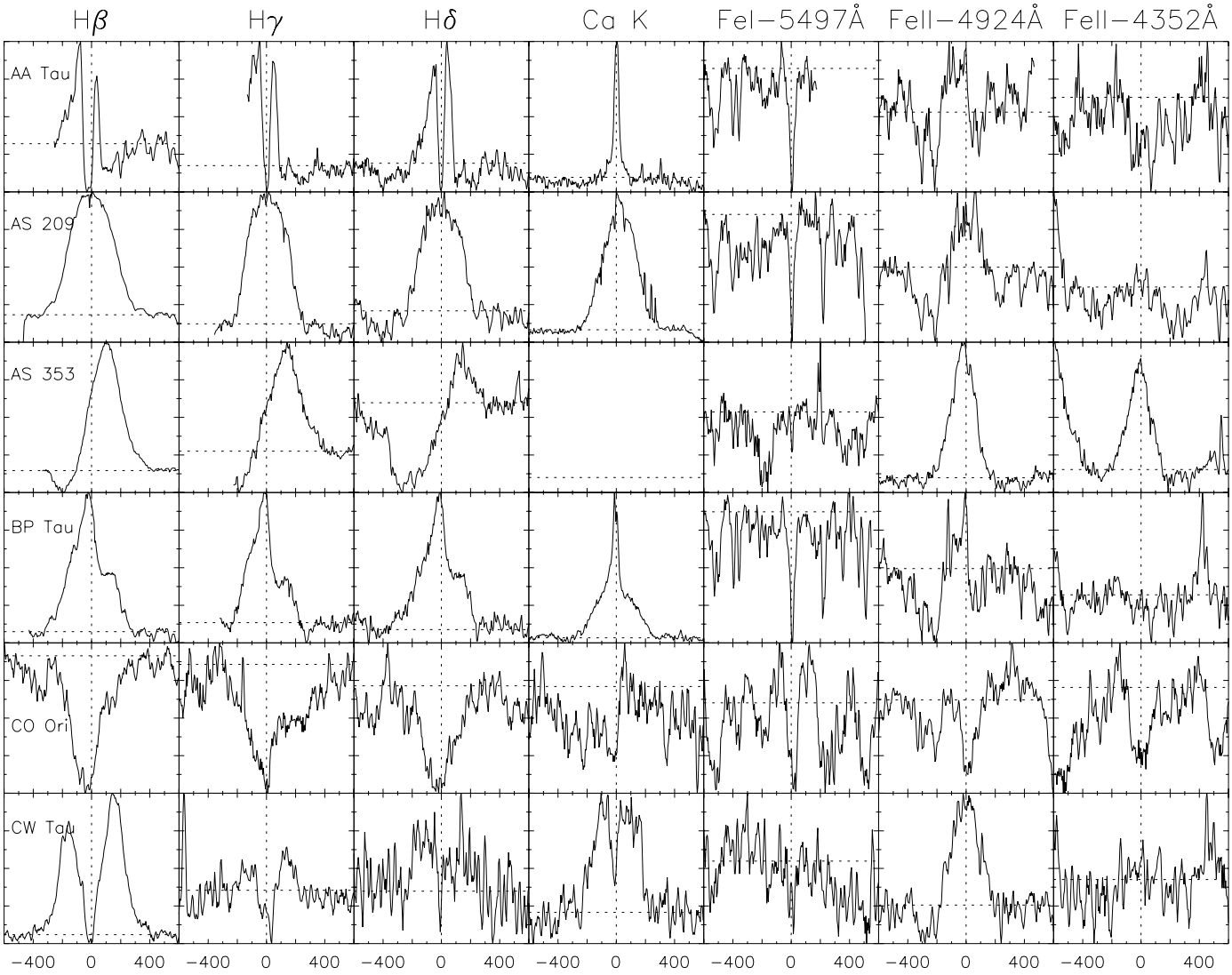

FIG. 1.—*Continued*

Mathieu 1997); the chosen spectrum corresponds to an outburst event when the lines are stronger and to a phase ($\phi = 0.02$) where there is no separation between the lines of the two components.

3. MEASUREMENTS

3.1. *Equivalent Widths and Profile Decomposition*

We first measure the equivalent width of all the lines in Figure 1 that could be reliably identified. The results are presented in Table 1 and will be used in the following sections to study the relations between "fluxes" (veiling-corrected equivalent widths) from different lines and between fluxes and parameters such as the mass-accretion rate.

The line profiles were also decomposed with a multiple Gaussian procedure based on the Marquardt method, so that we could also study correlations between line components. Most of the lines were very well fitted by one or two Gaussians and only sometimes required a third component. Some exceptions are the flat-topped profiles of T Tau, SU Aur, and DE Tau, which are clearly non-Gaussians. The fitting procedure was not always straightforward, since some lines are contaminated by nonstellar emission, some are blended by other lines, and some can be fitted with more than one Gaussian combination (such as two emissions instead of one emission and one absorption, for example). We explain below how we dealt with those problems.

The Hα line often exhibits a double-peaked profile, which in most cases was better fitted by a broad emission and a blue absorption than two emissions. The Hα wings are not steep and seem to belong to a very broad emission line rather than to two narrow ones. It is often possible to confirm that a true absorption is present by looking at the upper Balmer lines, where the feature is enhanced relative to the emission and dips below the continuum.

The Na D lines are strongly contaminated by the vapor lamps of the city of San Jose but our decomposition procedure was able to reliably subtract that contamination with a simultaneous Gaussian fit while decomposing the line profiles.

The Ca II and He I lines exhibit profiles typically with narrow and broad emission components; some lines show only one of the components. In some Ca II lines the narrow component is present inside a photospheric absorption core and, in that case, the emission-line equivalent width was measured from the base of the absorption core instead of the continuum. The Ca II infrared triplet (IRT) lines are also

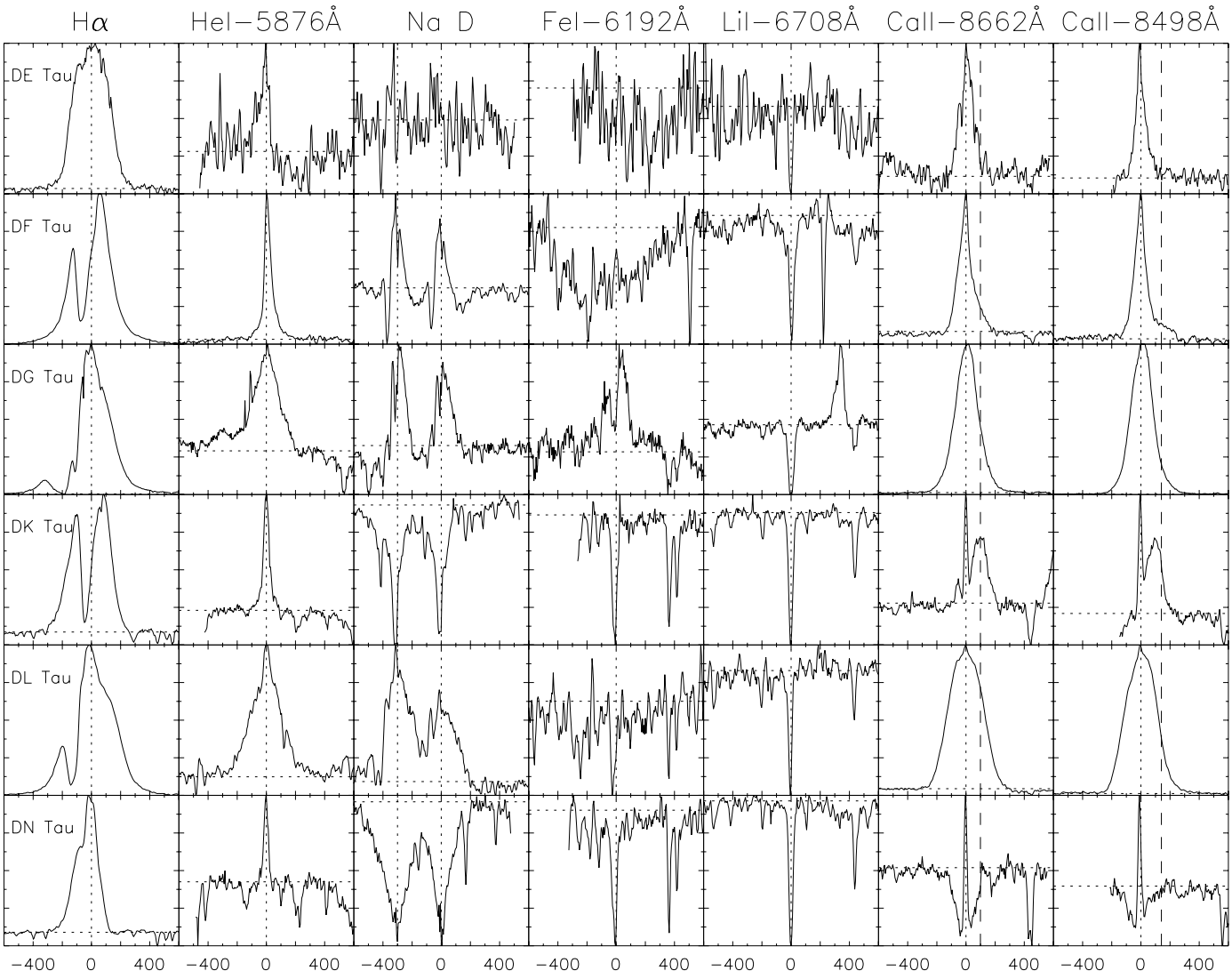

FIG. 1.—*Continued*

blended with a Paschen emission line, which usually has strengths less than 20% of the IRT, as also noted by Hamann & Persson (1992). Whenever the Ca II lines are weak or narrow, the Paschen contamination is significant and has been extracted from the equivalent width measurements.

Finally, the Fe II equivalent widths were only measured when the line was in strong emission and could surely be distinguished from the lines nearby.

3.2. *Veiling*

The equivalent widths presented in Table 1 are contaminated by the variable continuum against which they were measured. They need to be corrected for the veiling in order to represent a true emission strength that can be regarded as a "flux" measurement. Some of our spectra have measured veilings in previous papers (Basri & Batalha 1990; Johns-Krull & Basri 1997) but in order to be consistent we decided to measure all the veilings again. The new values are presented in the last columns of Table 1, and the common measurements agree within the errors with the previously published ones.

In order to calculate the veilings we chose spectral orders with many photospheric absorption lines, both in the blue and red settings. The red orders correspond to the wavelength ranges 5557 Å $< \lambda <$ 5642 Å and 5668 Å $< \lambda <$ 5755 Å and the blue orders to 4571 Å $< \lambda <$ 4641 Å and 4763 Å $< \lambda <$ 4836 Å. The idea is to compare the spectrum of a CTTS with that of a standard star with the same spectral type that has been broadened to the CTTS rotational velocity and veiled. The choice of suitable standard stars is important, and we followed, whenever possible, the suggestion of Basri & Batalha (1990) to use the Hyades dwarfs as reliable standards. We also used the standard and CTTS spectral types determined by them.

We first rotationally broadened the continuum-normalized spectrum of the standard star and then applied the veiling to the standard's spectrum, comparing it with the observed CTTS spectrum until a good match was found. The best adjustment was determined by eye, but a unique veiling value did not perfectly match all the photospheric lines and the results presented in Table 1 correspond to a mean value obtained with all the lines in the selected orders. The errors in the veiling determination are bigger for the higher veiling values, as the photospheric lines of highly veiled stars are extremely shallow and hard to match. Typically, we have errors of 0.1 for veilings smaller than 1.0 and up to 0.5 for the higher ones. Most of the rotational veloci-

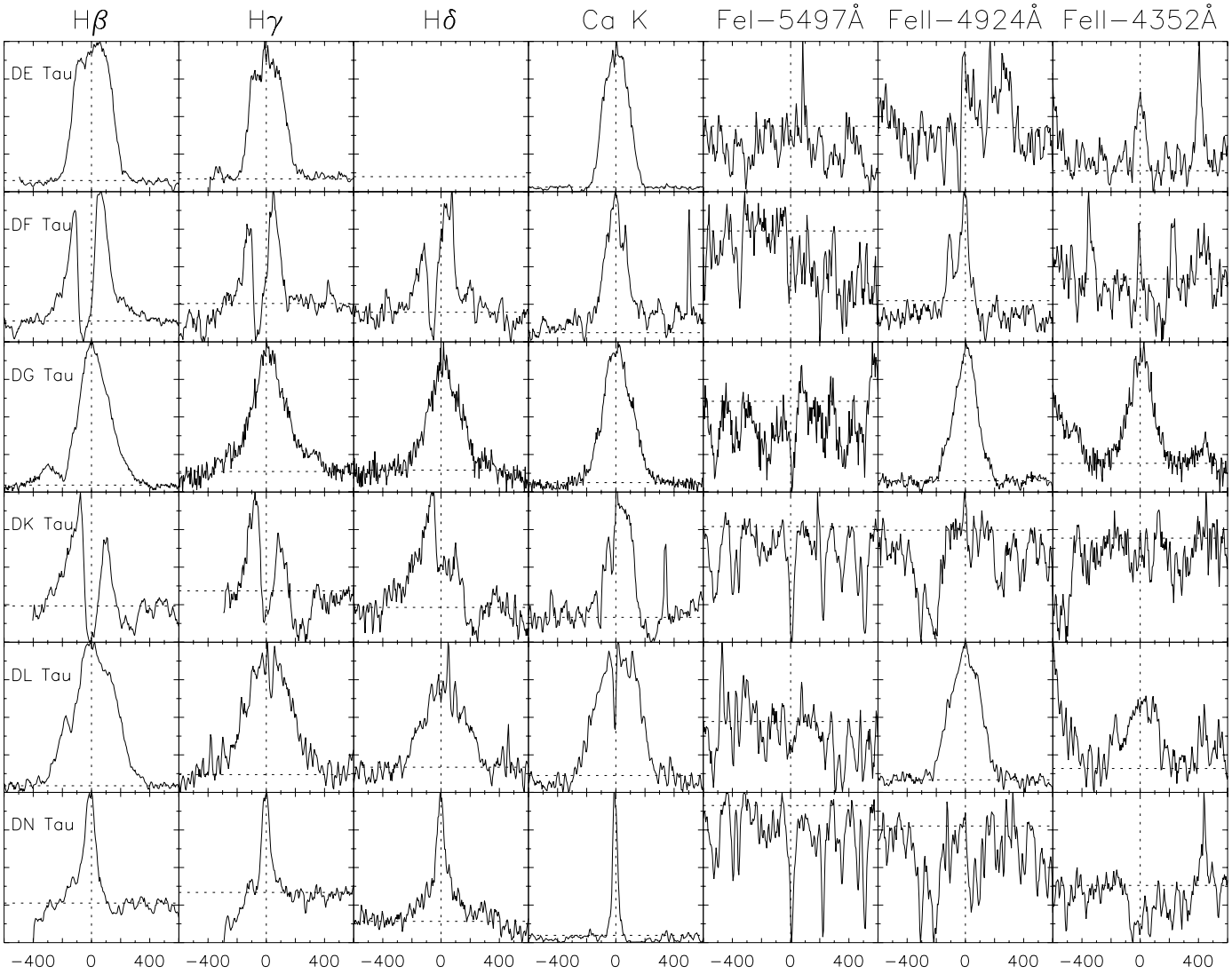

FIG. 1.—*Continued*

ties were taken from Basri & Batalha (1990), although we verified them by checking the match between the FWHM of the cross-correlation normalized profiles of the original standard with the CTTS spectra and of the original standard with the broadened and veiled standard.

The veiling values obtained are used to search for correlations between veiling-corrected line equivalent widths, defined as in Johns-Krull & Basri (1997):

$$W^0_{\rm eq} = W_{\rm eq}(V + 1)\,, \qquad (1)$$

where $W_{\rm eq}$ is the measured equivalent width and V is the veiling.

4. ANALYSIS

4.1. *General Characteristics*

The magnetospheric accretion model is the current consensus model to describe the accretion processes in CTTSs. These models predict general trends, such as central or blueshifted asymmetric broad emission lines, sometimes with redshifted absorption components (Hartmann et al. 1994; Muzerolle, Calvet, & Hartmann 1998b), that we should be able to verify in our large sample of stars and lines. The magnetospheric accretion scenario may also include winds that would cause further emission and blueshifted absorption (Shu et al. 1994). Some theoretical predictions have been confirmed by observational results (Edwards et al. 1994; Muzerolle et al. 1998a), but there is still a long way to go in order to fully understand the nature of the processes taking place in CTTSs. Below are some general profile characteristics from our sample of stars that we will analyze in detail in the next sections.

Many of our emission lines show broad components (BC) that tend to have blueshifted centroids (Hα, Hβ, the He I BC, the IRT BC, Na D, and Fe II λ4923) following the magnetospheric predictions, but the centroids are also redshifted in some stars and exhibit a wide range of shift values. The broad emission components are also generally well fitted by Gaussians, which may have a turbulent origin (Basri 1990) rather than the infall scenario. Redshifted absorption is not commonly present. The clearest example is BP Tau, where it appears in the Balmer lines, the Na D, and the Ca II (λ8662). Blueshifted absorption is a much more common feature that can be seen in many Balmer and Na D lines and sometimes in lines such as Ca K in RW Aur. Many lines show a multiple-component profile that can often be decomposed either as narrow and broad components, e.g., He I, Ca, and Fe lines (Basri & Batalha 1990;

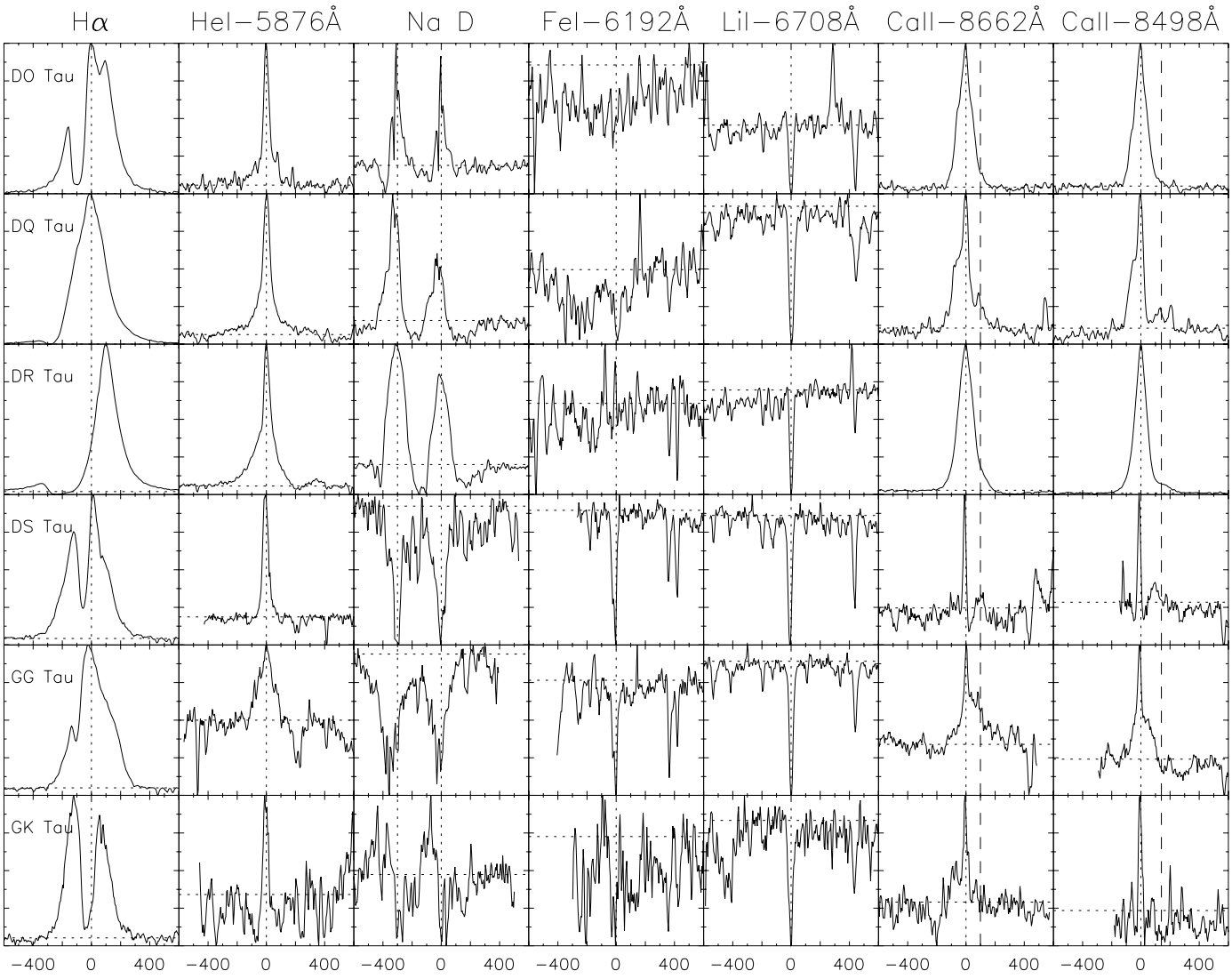

FIG. 1.—*Continued*

Beristain, Edwards, & Kwan 1998), or as emission and absorption components, such as the Balmer lines. The different components often show distinct characteristics (such as broadening and shifts), suggesting that the lines may originate in distinct regions. The Fe I lines are mostly in absorption but can be found in strong emission in very active stars (as in AS 353, DG Tau, and RW Aur) always with a double-peaked profile that could be due to NLTE chromospheric core inversion (inversion of the source function) or disk rotation.

4.2. *Line Strengths*

The study of the correlations between the fluxes of different lines is an important tool that gives insight on the relations between different line formation regions. Correlations can indicate common forming regions, but they can also mean that a common process is affecting both regions at the same time. In this section we discuss the correlations that appear in our data, as well as those that do not.

The Balmer lines emission components are well correlated with each other, as are the IRT lines with each other, which is expected as they should be formed in regions with the same physical characteristics. The difference between them should arise mainly because of differences in line optical depths. In the Balmer lines case, the correlation seems to decrease as we compare lines that are farther apart in the series; e.g., Hα and Hβ show a strong correlation with each other (Fig. 2, *top*) with a false alarm probability (FAP) of 3.24×10^{-7}, but Hα and Hδ do not (FAP = 0.168). This behavior is biased by stars with strong wind contribution, where the emission component is sometimes almost absent because of large absorption components and/or a hot underlying photosphere. By eliminating those stars, the good correlations are partially recovered (Fig. 2, *bottom*), with the FAP of the Hα and Hδ emission components decreasing to 3.55×10^{-4} and presenting a linear correlation coefficient $r = 0.880$.

The entire Hα and He I lines are also well correlated (Fig. 3; FAP $= 1.26 \times 10^{-6}$), except for DQ Tau, which has a very high Hα equivalent width in the outburst spectra we chose, and CW Tau, which has a high uncertainty in the veiling measurement (we get FAP $= 4.65 \times 10^{-10}$ without DQ Tau and CW Tau). The same kind of correlation is verified with Hβ, but Hγ and Hδ do not show a well-defined correlation with He I. The apparent lack of correlation with Hγ and Hδ may be due to the small number of spectra

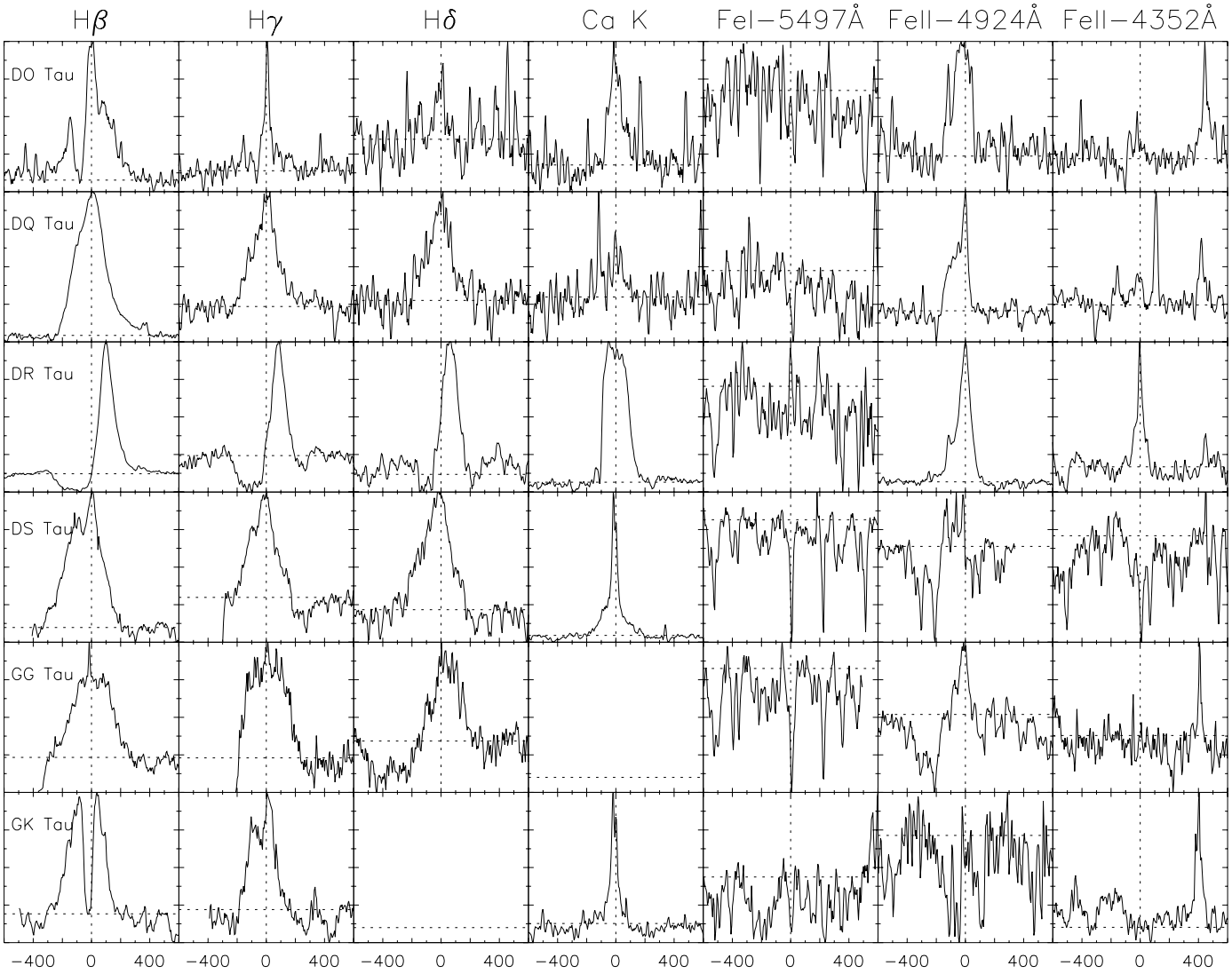

FIG. 1.—*Continued*

where those lines could be reliably measured and the lower signal to noise present in our spectra in that region. Apart from the correlation with the entire lines, we also verified a good correlation between the Hα emission component and the He I BC (FAP = 4.68×10^{-4} with DQ Tau and CW Tau and FAP = 8.32×10^{-6} without them). The He I line is believed to form in high-temperature regions (20,000 to 50,000 K), and, together with the large width of its BC, it suggests that the BC comes either from the highly turbulent shock region or the magnetospheric flow, where the broad emission component of the Balmer lines is also supposed to be formed. Due to their larger optical depths, the Balmer lines probe a much larger volume of gas than the He I lines, but the correlations between the entire lines and the components show that their formation regions are strongly related to each other.

Also thought to be formed in the accretion flow, because of its large widths and blueshifted center, the broad IRT component does not strongly correlate with the He I BC (FAP = 1.97×10^{-3} and $r = 0.678$ for $\lambda 8498$) or with the Hα emission (FAP = 6.12×10^{-3} and $r = 0.590$ for $\lambda 8498$). For the He I BC, no correlation is found for small equivalent width values and a tendency for the equivalent widths to increase together exists, although with much scatter. For the Hα, however, a correlation seems to exist, except for the higher Hα flux values (where the scatter is really large). Although the Ca II line is formed at much lower temperatures, it is expected to strongly correlate with Hα and He I, if the accretion flow is sufficiently organized that a global change in accretion rate is felt by all diagnostics.

Batalha et al. (1996) showed that the narrow components (NC) of CTTSs have a flux excess when compared with the WTTSs, and this was attributed to the reprocessing of radiation produced in accretion shocks as the accreting material hits the stellar atmosphere. However, neither the He I NC nor the Ca II NC correlate with the Balmer emission, which implies that although both the NCs and the Balmer lines are related to accretion, they are probably probing regions that are far away from each other and consequently not equally influenced by the same physical processes, or the time delay for changes that affect one region to reach the other is too large for the changes to show up in simultaneous spectra of both components.

We also confirmed the trend noticed by Batalha et al. (1996), that the IRT and the He I NCs are positively correlated (Fig. 4 and FAP = 1.41×10^{-5}; unsurprisingly, since

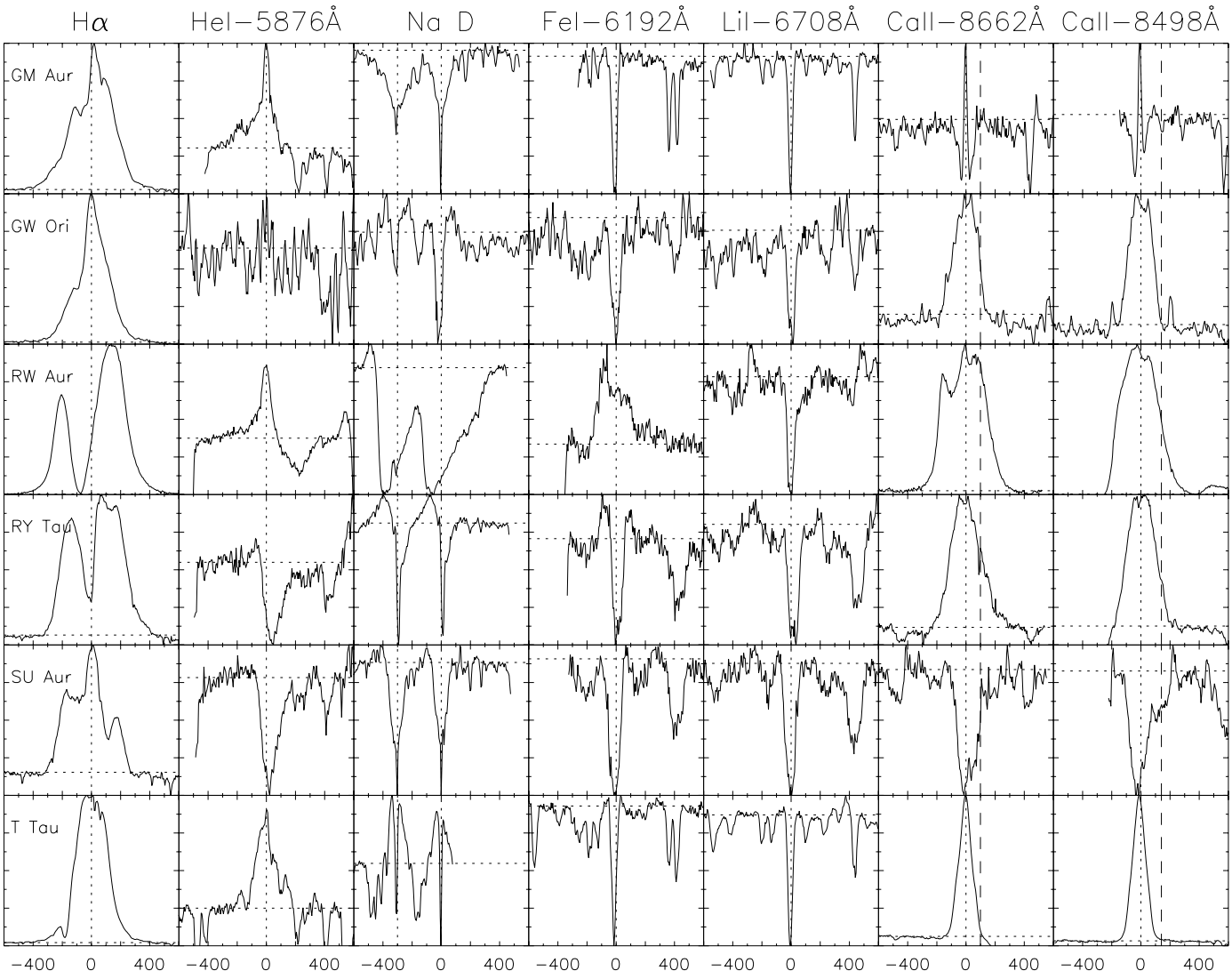

FIG. 1.—*Continued*

we have a lot of data in common), while Muzerolle et al. (1998a) found that they were uncorrelated. Those lines are generally thought to sample quite different temperature regions—the He I is formed in high temperatures ($>20{,}000$ K) while the IRT is a chromospheric line formed at 4000 K $< T <$ 7000 K. The correlation found is probably related to the excess emission due to the influence of the accretion shock on the stellar atmosphere, a common feature in both of them.

Iron lines are quite common in CTTSs, so we decided to analyze the behavior of four of them (two Fe I and two Fe II) in our sample. The Fe II (λ4923) line was only fitted when in emission. Only 40% of the sample presented this line in emission, and we were able to measure the veiling for just some of them, but before applying the veiling corrections it shows a good correlation with the He I BC and with the IRT BC. These correlations may indicate that the Fe II lines, at least when in strong emission, share a common emitting region with the BCs of He I and the IRT.

The Fe I absorption lines (λ6192 and λ5497), with excitation energies of 4.43 eV and 3.27 eV, respectively, are not correlated with each other. Although visually they both have some resemblance to the Li I line, nothing was found between the Fe I (λ6192) and Li I, while a strong correlation exists between the Fe I (λ5497) and Li I lines. This is due to a temperature effect: the cooler stars show the deepest lines.

Another important aspect of the correlation measurements is the quest for good accretion rate indicators that would later provide an easy way to obtain these rates for other stars. Using the mass-accretion rates in Hartmann et al. (1998), there is a very good correlation between the IRT veiling-corrected equivalent widths (Ca II λ8498 and λ8662) and mass-accretion rates (Fig. 5, *top*, and FAP $= 1.80 \times 10^{-4}$), as in Muzerolle et al. (1998a) for Ca II (λ8542). The only exception is DQ Tau, which has a $\log \dot{M} = -9.4\ M_{\odot}\ \mathrm{yr}^{-1}$, according to Hartmann et al. (1998), but $-7.3\ M_{\odot}\ \mathrm{yr}^{-1}$ according to Hartigan, Edwards, & Ghandour (1995) (the largest discrepancies between their values). DQ Tau is known to have a variable accretion rate that depends on the orbital phase of the binary system and on events such as outbursts that may occur when the stars approach each other (Basri et al. 1997). We decided not to use this star.

The Balmer lines and their components are also correlated to the mass-accretion rates (Fig. 5, *middle and bottom* with FAP $= 3.40 \times 10^{-4}$ and 7.09×10^{-3}, respectively).

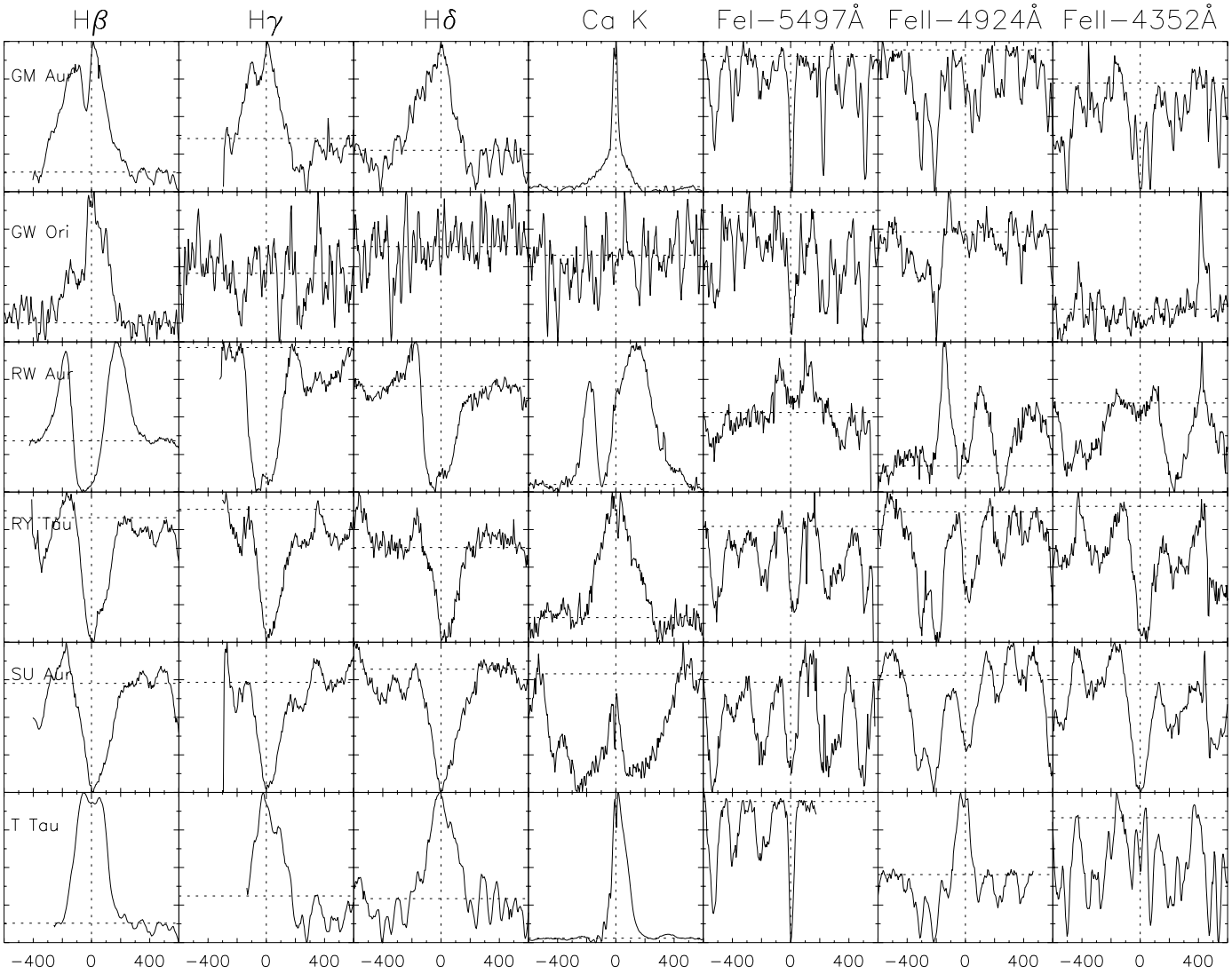

FIG. 1.—*Continued*

The results for the absorption component are not as reliable as the others, mainly because of the small number of stars that exhibit a clear absorption and for which there are published mass-accretion rates. The flux of the emission and absorption components increases as the accretion rate increases, showing that the accretion may be powering both the emission and the outflow. This would be consistent with theoretical results (Shu et al. 1994) that suggest that the wind mass-loss rate and the disk-accretion rate are directly proportional (but see below for caveats).

4.3. *Evidence for Outflows*

Winds are expected to be present in CTTS and help carry away angular momentum. If cool, they should appear mainly as absorption components. Due to the presence of the disk the absorption is expected to be blueshifted; the receding part of the wind is blocked by the disk from the observer's line of sight. The emission components of CTTS were thought for some time to be produced in optically thick winds, but these models also generated upper Balmer line profiles with very deep absorptions that were not consistent with observations.

The Balmer and Na D blueshifted absorption components are the clearest evidence in Figure 1 that a strong wind is present in our sample of CTTSs. Almost 80% of our stars show blueshifted absorption components in at least one line, the most common being Hα (see Table 2 for Hα and Tables 2 and 3 for a complete listing). The number of blueshifted components decrease as we look at the upper Balmer lines, appearing only in about 35% of the Hδ profiles (where they tend to be weak). This suggests that the blueshifted absorptions arise from a region that is optically thin, at least in the upper Balmer lines, and distinct from the emission component that is believed to arise mainly in the optically thick accretion flow. Some stars, like DR Tau and AS 353, present P Cygni profiles in all the Balmer lines. These are normally associated with strong winds, and other stars, such as CO Ori, RW Aur, SU Aur, and RY Tau, have such a strong absorption component that it sometimes suppresses the emission in the upper Balmer lines of the stars with the hottest underlying photospheres. A number of these stars are known to be jet sources.

The eight stars in our sample that exhibit blueshifted absorption components in the Na D lines (presumably indicating high mass-loss rates; Hartmann 1998) also do in Hα. The lack of P Cygni profiles in the Na D lines does not necessarily mean low mass-loss rates, as the star may present a deep photospheric absorption that prevents the

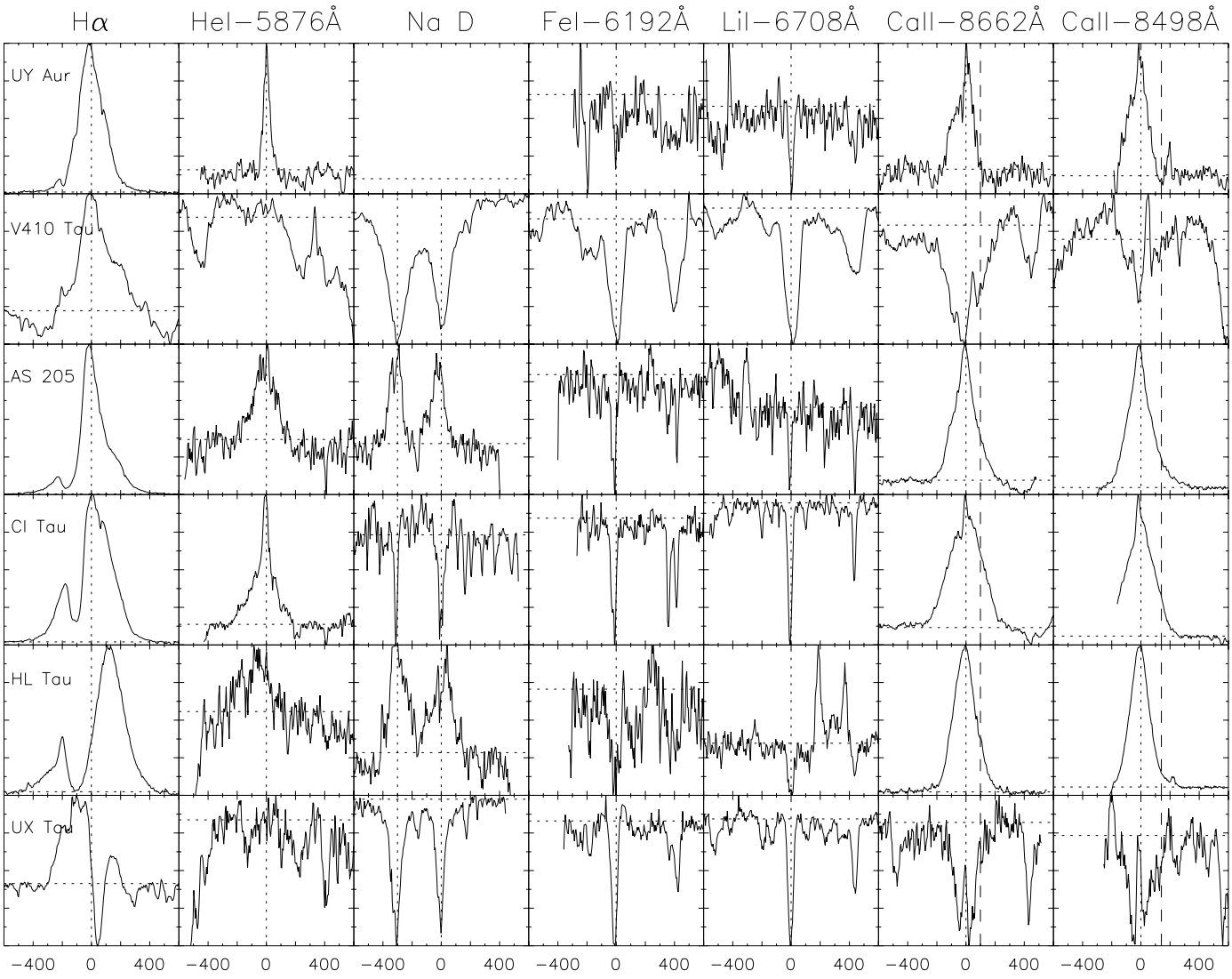

FIG. 1.—*Continued*

detection of the blue absorption due to the wind (Natta & Giovanardi 1990). Due to the difference in their optical depths, the Balmer and Na lines will sample different wind volumes. As resonance lines, the sodium probes the coolest part of the wind. The blueshifted components of both lines tend to be centered at approximately the same velocities (Tables 2 and 3), likely meaning that different wind regions share some common kinematic component. The Na D blueshifted absorptions bear no other resemblance to the Hα ones, being much weaker in intensity and width. The position of blueshifted absorption centers in these lines vary from star to star, suggesting that the wind velocities can occur with a wide range of values (from 0 to -270 km s^{-1} in our sample; see Fig. 6). There may well be projection effects that must be taken into account; these would imply the outflow is not spherical.

After decomposing the profiles we can also investigate the correlations that appear between different wind components and between wind components and other features in order to better understand the wind-forming region. The Hα and Hβ blueshifted absorptions are very well correlated (FAP $= 2.39 \times 10^{-8}$), showing that they both probe the same wind region, and although there is apparently no correlation with the blueshifted absorptions of Hγ and Hδ, this may be due to the small number of cases. Where the absorption does appear in the upper lines, the wind component is often very weak and consequently hard to fit.

The Hα and Hβ blueshifted absorptions also show some correlation with their line's emission components: the stronger the emission, the stronger the absorption. Unfortunately, that does not have a unique interpretation. One possibility is that the same mechanism that is powering the emission is also powering the wind in the sense that when more material is accreted there is more to outflow. This is predicted by the accretion model and also means that the absorption region is outside the emission region. A second possibility is that if both emission and absorption were formed in winds, the absorption component would be due only to the decay of the source function in the outer regions of the atmosphere and not to the accretion itself. If the first possibility is correct, this relation could also explain the trend seen between the Hα emission and absorption components and the mass-accretion rates.

Finally, the present result may also be an effect of line optical depth; if the wind is optically thick the central depth of the blueshifted absorption is fixed and the changes that

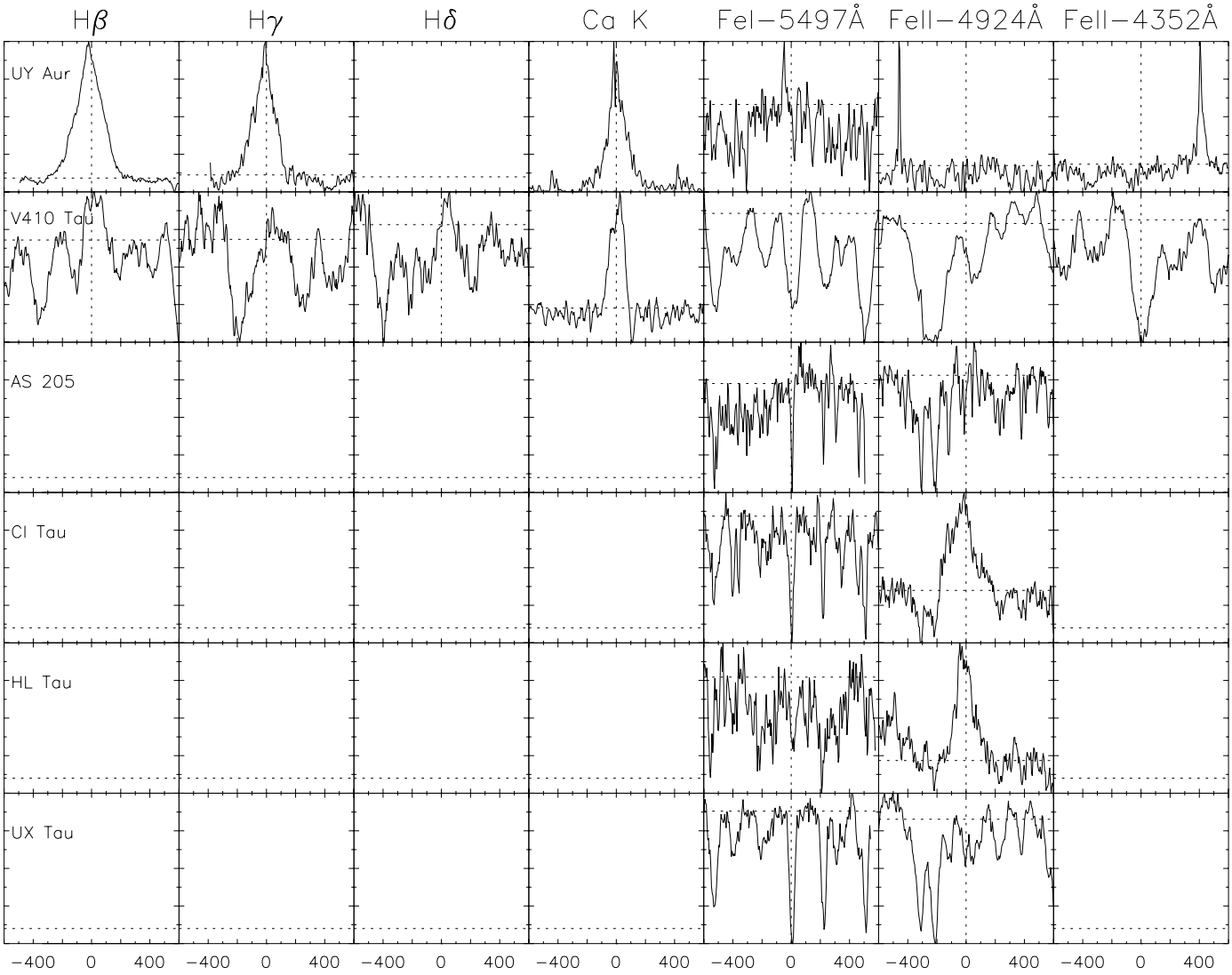

FIG. 1.—*Continued*

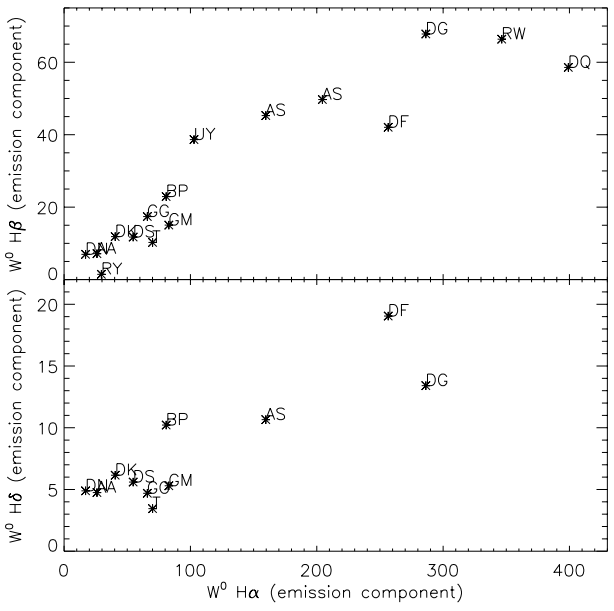

FIG. 2.—Veiling-corrected equivalent widths of emission components: $W^0_{H\alpha}$ vs. $W^0_{H\beta}$ and vs. $W^0_{H\delta}$.

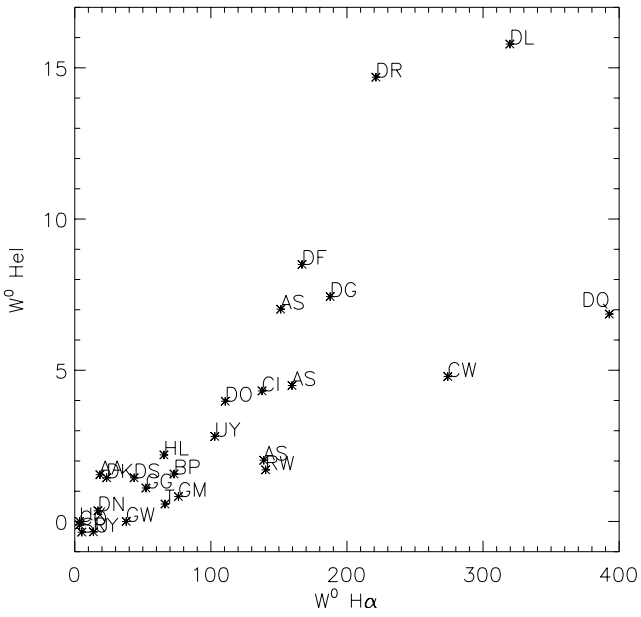

FIG. 3.—$W^0_{H\alpha}$ vs. W^0_{HeI}

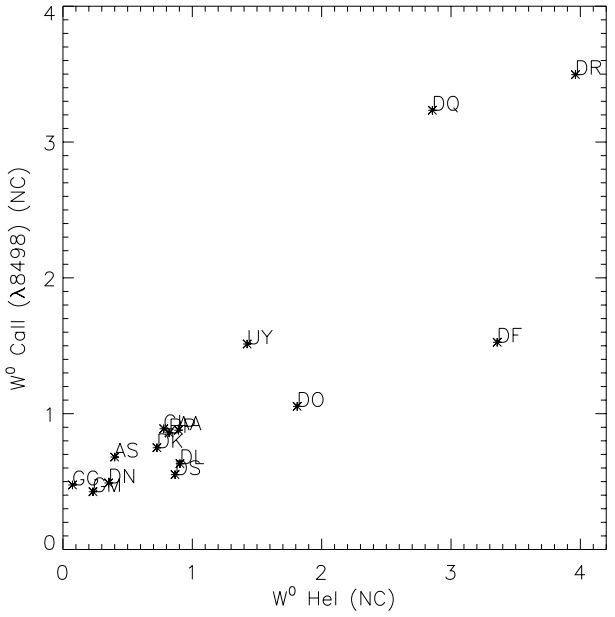

FIG. 4.—$W^0_{\text{He I}}$ (NC) vs. $W^0_{\text{Ca II}(\lambda 8498)}$ (NC)

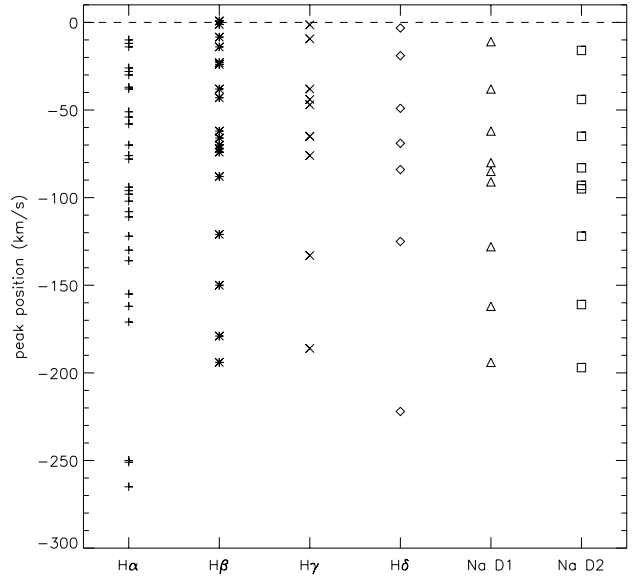

FIG. 6.—Blueshifted absorption component's peak position

appear are in fact only due to the emission component variations as shown by Johns & Basri (1995b) in the case of SU Aur. Johns-Krull & Basri (1997) also found that the Hα absorption and emission strengths of many DF Tau spectra were correlated and that the absorption component strength correlated with the veiling.

A curious fact about the absorption components can be noticed in the stars that show an absorption component in the four analyzed Balmer lines. This component tends to be shifted toward the red as we go from Hα to Hδ, and in Figure 7 we plot the absorption centers versus the Balmer lines oscillator strengths for those stars. It seems that we may be seeing the acceleration of the flow. This shift of the absorption component can also be noticed in Edwards et al. (1994) in the residual profiles of DK Tau and in Appenzeller, Reitermann, & Stahl (1988) in the DR Tau spectra, showing that this behavior may be quite common among CTTSs.

Another feature that is associated with strong activity, presumably both inflow and outflow, concerns the iron lines in strong emission. These lines are often in absorption in our sample, but Fe II (λ4923) is also found in emission in about 40% of our stars. When this happens, a wind component is present at least in Hα, sometimes also in the other

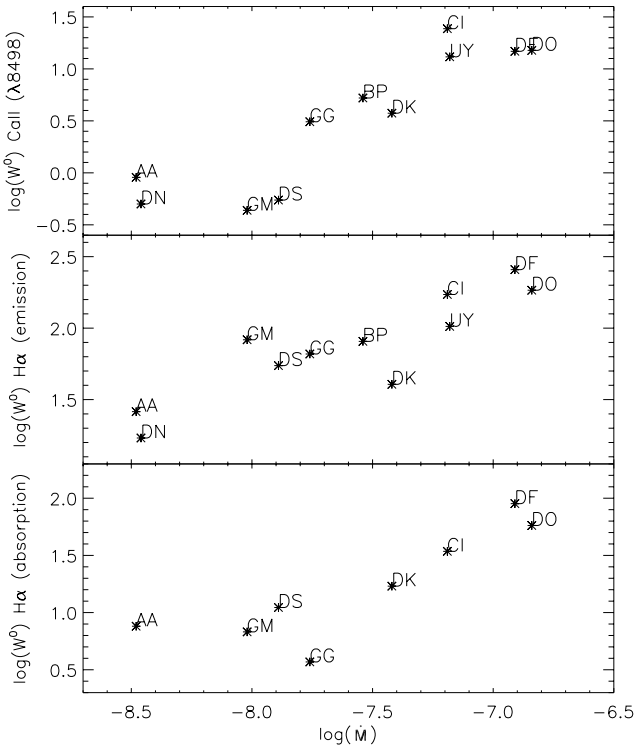

FIG. 5.—$\dot{M}$ vs. $W^0_{\text{Ca II}(\lambda 8498)}$ and vs. $W^0_{\text{H}\alpha}$ (emission and absorption components).

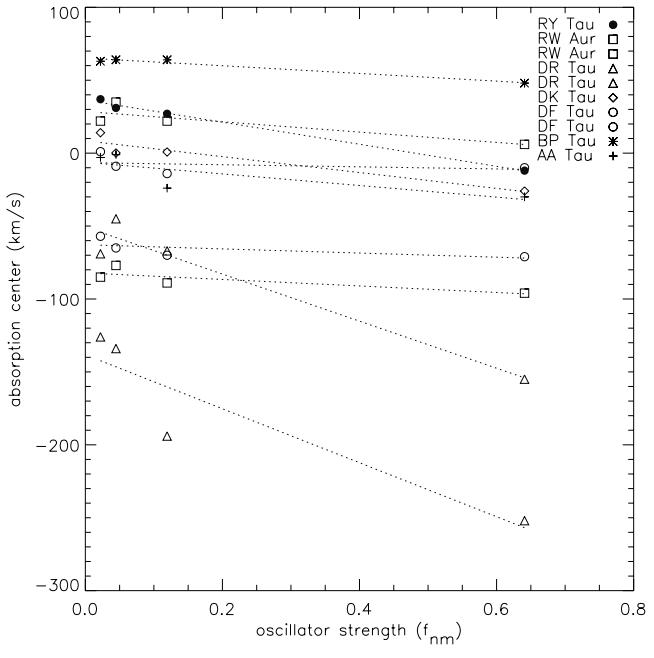

FIG. 7.—Balmer line absorption center vs. oscillator strength. RW Aur, DR Tau, and DF Tau are plotted twice as two wind components were measured.

TABLE 2

VELOCITY CENTROID (km s^{-1}) OF LINE PROFILE COMPONENTS

	Hα			Hβ			Hγ			Hδ			He I	
STAR	c1	c2	c3	c1	c2	c3	c1	c2	c3	c1	c2	c3	NC	BC
AA Tau.....	−30.1*	−34.1	x	−23.9*	−26.9	87.9*	−1.4*	−13.1	103.5*	−3.2*	0.3	101.0*	−0.4	9.0
AS 205.....	−109:*	−46.4	174.5										x	−14.3
AS 209.....	−4.7	x	x	1.3:	x	x	8.1	x	x	−1.4	x	x	−4.2	0.6
AS 353.....	−137:*	−266:*	30.1	−179.2*	97.7	x	−186:*	131.6	x	−222.5*	136:	x	x	−41.2
BP Tau	4.4	48.1*	x	−6.1	63.8*	x	−0.9	63.8*	x	−4.5	63.4*	x	0.4	−10.5
CI Tau.....	−98.3*	−9.2	x										−5.1	−23.0
CO Ori	−37.0*	−111.6*	22.7	−38.1*	x	x	−38.4*	115:*	x	−19.9*	x	x	6:*	x
CW Tau	−14.3*	−130.9*	−0.8	−1.2*	8.3	x	x	x	x	x	x	x	x	−58.0
DE Tau	−0.4	x	x	12.3	x	x	8.2	x	x				−2:	−53:
DF Tau	−70.8*	−10.4*	−5.3	−70.2*	−14.2*	−17.9	−65.3*	−9.4*	−28.3	−57.3*	1.0*	−22.3	4.6	21.8
DG Tau	−102.9*	−162.2*	−38.4	−150.1*	−50.1	x	17.7	x	x	21.0	x	x	x	−4.2
DK Tau	−26.3*	−13.7	x	0.8*	−14.3	213.8*	0.1*	−7.8	234.1*	14.2*	−30.6	213.6*	−0.2	0.4
DL Tau	−122.0*	2.1	59.1*	−121.4*	8.3	x	14.7	x	x	21.0	x	x	4.2	−2.5
DN Tau	−58.2*	−38.8	x	−43.1	−7.7	149.3*	−2.4	x	x	0.9	−3.2	x	−2.8	x
DO Tau	−76.0*	−3.3	43.1*	−72.1*	−6.3	50.7*	x	x	x	x	x	x	−0.5	5.6
DQ Tau	−250.0*	−8.2	262.9	−7.2	297.	x	−6.7	x	x	−12.1	x	x	2.3	−4.2
DR Tau	−155.0*	−251.8*	100.9	−66.8*	−194.0*	100.6	−44.7*	−133.8*	81.2	−69.3*	−125.8*	58.3	0.1	−14.5
DS Tau.....	−54.8*	−35.4	x	−62.1*	−49.4	x	−65.7*	−28.3	x	−33.9	x	x	−7.4	6.0
GG Tau	−94.8*	14.9	57:*	6.1	x	x	10:	x	x	42.2	x	x	3.0	−5.1
GK Tau	−28.3*	−33.3	x	−24.4*	−32.0	x	x	x	x				−4.7	x
GM Aur....	−51.8*	7.5	x	−43.7*	−49.7	x	−45.9*	−33.4	249.3*	−40:	189:*	x	2.4	−17:
GW Ori	−78.7*	−5.2	x	−74.4*	−22.6	x	x	x	x	x	x	x	x	x
HL Tau	−38.7*	−2.3	x										x	x
RW Aur	−96.0*	4.5	5.7*	−88.7*	9.5	21.6*	−76.8*	34.9*	x	−84.6*	−72:	21.8*	0.5	−15.0
RY Tau.....	−12.2*	14.3	118.*	28:*	x	x	31:*	x	x	36.7*	x	x	54:*	x
SU Aur	−22.4	10.7	103.1*	38.9*	x	x	20.4*	x	x	23.6*	x	x	29.2*	x
T Tau.....	−171.*	−2.68	x	−4.3	x	x	9:	x	x	2.7	x	x	x	−9.3
UX Tau	−48.8	42.5*	269.4*										x	x
UY Aur	−30.6	5.4	x	−15.0	−21.9	x	−18.3	−7.7	x				0.1	10.1
V410 Tau...	60.7	102:*	x	x	x	x	x	x	x	x	x	x	x	x

NOTE.—Lines for which the cell is left blank were not available, and those marked with an "x" were not present or could not be reliably measured in the observed spectrum. Velocities marked with an asterisk represent absorption components. The notations c1, c2, and c3 represent the emission and absorption components of the lines that could not be decomposed as NC and BC.

TABLE 3

VELOCITY CENTROID (km s^{-1}) OF LINE PROFILE COMPONENTS (CONTINUED)

	Na D1			Na D2			Fe I λ6192	Li I λ6707	Ca II λ8662			Ca II λ8498			Ca K		Fe I λ5497	Fe II λ4924	Fe II λ4352
STAR	c1	c2	c3	c1	c2	c3	c1	c1	NC	BC	c3	NC	BC	c3	NC	BC	c1	c1	c1
AA Tau.....	4.3*	x	x	−4.4*	x	x	−13.1*	−5.4*	−3.3	x	x	−14:	x	x	2.3	−5.7	5.6*	x	x
AS 205.....	−12.4	x	x	−28.2	x	x	−16.3*	−7.5*	−6.1	−9.7	375.1*	−15.4	−7.8	x			5.9*	x	
AS 209.....	11.4	x	x	11.0	x	x	−15.0*	−5.2*	−10.0	4.6	x	−20.0	−6.4	x	x	25.7	4.8*	x	x
AS 353.....	−197.1*	−28.3	x	−194.4*	16.3	x	0.7	−2.9*	x	0.3	x	x	−10.6	x	x	x	x	−21.4	−14.4
BP Tau	62.9*	x	x	53.7*	x	x	−10.4*	−1.6*	−1.8	0.4	37.9*	−2:	25:	x	−7.7	−9.0	7.5*	x	x
CI Tau.....	x	x	x	x	x	x	−16.0*	−6.9*	−3.6	−1.0	x	−16.4	−4.5	x			2.5*	−27.5	
CO Ori	−44.8*	−13.4 *	x	−38.5*	−5.2 *	x	−9.3*	3.2*	x	x	x	x	−66.0	−3.0*	x	x	11:*	x	x
CW Tau	x	x	x	x	x	x	−5.7*	1.6*	x	4.6	x	3.4	13.0	x	−11.1*	−3.7	x	−0.4	x
DE Tau	x	x	x	x	x	x	x	−2.8*	6.9	6.8	x	−10.8	1.5	x	x	3.4	x	x	2.4
DF Tau	−65.2*	−13.1	141.6	−62.2*	−23.2	136.4	x	4.1*	−1.4	−11.7	x	−0.7	−7.2	x	−5.7	−1.6	x	−7.5	−5.5:
DG Tau	−95.4*	−6.8	x	−91.9*	6.9	x	−2.5	−0.2*	x	4.9	x	x	8.2	x	x	10.2	7.2*	2.9	5.9
DK Tau	−16.3*	x	x	−11.9*	x	x	−11.3*	−2.2*	−1.4	93.7	x	−5.3	91.2	x	200:*	32.6	6.7*	x	x
DL Tau	−122.7*	−18.1	x	−128.1*	13.2	x	−20.1*	−6.2*	−3.5	−1.6	x	−6.0	2.9	x	x	15.1	x	−1.8	x
DN Tau	−8.9	x	x	1.9	x	x	−10.9*	−0.8*	−2.7	x	x	−9.1	x	x	−5.5	x	8.0*	x	x
DO Tau	−84.6*	−4.2	x	−80.0*	1.0	x	x	−0.2*	−3.3	−6.4	x	−5.1	−3.6	x	x	−3.1	x	−20.3	x
DQ Tau	−24.4	100:*	x	−23.6	101:*	x	9.1*	4.0*	0.3	−45.6	x	−1.4	−54.9	x	x	x	x	−0.2	x
DR Tau	−9.74	162.9*	x	−4.14	108.7*	x	x	−1.3*	x	−2.5	350.7*	x	−4.4	x	x	−3.1	x	−1.7	−2:
DS Tau.....	−4.1*	x	x	−4.0*	x	x	−11.6*	−7.9*	−9.7	x	x	−11.9	x	x	−10.4	−19.3	7.2*	x	x
GG Tau	x	x	x	x	x	x	−7.0*	1.0*	1.0	50.7	x	−10:	4:	x	x	x	8.2*	x	x
GK Tau	x	x	x	x	x	x	x	−1.7*	−4.8	−30:	x	−5:	x	x	−12.0	−42:	3.5*	x	x
GM Aur....	5.4*	x	x	0.8*	x	x	−11.0*	−4.3*	−3.0	x	x	−6.7	x	x	−4.1	−15.4	7.1*	x	x
GW Ori	−15.0	x	x	4.9	x	x	−2.8*	3.4*	x	−1.6	x	x	−1.6	x	x	x	12.0*	x	x
HL Tau	2.3	x	x	6.3	x	x	−8.6*	−0.6*	x	−10.1	x	x	−8.5	x			x	−11.9	
RW Aur	−93.0*	12.1*	x	x	−85.0*	10.7*	−13:	0.2*	x	x	x	x	−11.0	285.8*	−52.0*	37.3	x	x	x
RY Tau.....	27.2*	−98.0	x	40.4*	−84.2	x	9.1*	17.8*	x	−2.3	x	x	5.3	x	x	5.0	27.1*	x	x
SU Aur	−4.3*	x	x	0.2*	x	x	−11.8*	−3.4*	x	x	11.5*	x	x	−10.6	x	x	2.2*	x	x
T Tau	−161.6*	−7.76	x	−161.9*	−9.73	x	−14.6*	−5.4*	x	−4.46	x	−13:	−12:	x	x	25.2	5.7*	−16.4	x
UX Tau	−9.8*	x	x	−5.9*	x	x	−12.8*	−3.2*	−9.0	x	x	−13.1	x	x			6.3*	x	
UY Aur	x	x	x	x	x	x	x	2.6*	18.9	−35.6	x	0.9	−23.1	x	−10.6	10.4	x	x	x
V410 Tau...	5.2*	x	x	2.7*	x	x	−1.3*	7.8	49.2	x	x	46.5	x	x	5.2	x	10.5	x	22.8

NOTE.—Markings same as Table 2.

Balmer lines and in the Na D lines, and the IRT lines always show a BC. The Fe lines in emission seem to be related to both the presence of outflow and high veiling, as some stars that show blueshifted absorption in Hα but no BC in the IRT do not present Fe I (λ4923) in emission. DG Tau, AS 353, and RW Aur, that also exhibit Fe I (λ6192) and Fe II (λ4352) in strong emission, also have associated jets (Edwards et al. 1994; Mundt & Eislöffel 1998). But unlike the forbidden lines that tend to be blueshifted, the iron lines when in emission are centered at the stellar rest frame. They are probably not produced in the outflow (wind or jet), since the occultation of the receding part of the flow by the disk would yield a blueshifted line.

4.4. *Evidence for Infall*

Redshifted absorption components in the line profiles (inverse P Cygni profiles) can be the clearest spectral evidence that infall of material is occurring, and they are naturally predicted by the magnetospheric accretion models. These models, however, require special conditions for the redshifted absorption component to be visible, such as low line thermalization, low emission damping wings, and proper inclination values. The inclination dependence arises from the contrast of the line source function of the infalling gas and the continuum source function where the gas stream is projected (Hartmann et al. 1994). If the projection is against the cool photosphere (low inclinations) no absorption is found, but if it is against the hot shock material, such as a ring or spots (higher inclinations), the absorption can be produced.

Edwards et al. (1994) presented an analysis of 15 CTTSs included in our sample, and showed that 87% of their stars had redshifted absorption components in at least one line at approximately 200 to 300 km s^{-1}, a range of velocities that is consistent with the ballistic infall predicted by the magnetospheric models for a typical CTTS. Only about 40% of our stars have redshifted absorption components in at least one line and generally not at approximately 200 to 300 km s^{-1}. BP Tau, for example, shows redshifted absorption in many lines at about 50 km s^{-1} and UX Tau has a strong redshifted absorption in Hα at 43 km s^{-1}. The difference in the absorption centroid position of the stars from the values predicted by the models could partially be due to inclination effects. The difference in the number of redshifted absorption occurrences found in the two different analyses could be due to the fact that Edwards et al. (1994) analyzed residual profiles instead of the original ones. This gives, according to them, a high sensitivity in defining features such as the Balmer lines wings, where the redshifted absorption lies. However, in the residual profiles showed by Muzerolle et al. (1998a) of 11 CTTSs, redshifted absorption at typical free-fall velocities can be found in less than half of their sample, which is more in agreement with the predictions of the magnetospheric accretion models.

In order to compare our results with the ones cited above we decided to generate residual profiles from our sample, choosing eight lines commonly found in emission: Hα, NaD, He I, Ca II (λ8498 and λ8662), Hβ, Hγ, and Fe II (λ4352). Hδ was excluded as most of our spectra present low signal to noise in that region, making it hard to obtain reliable information about small absorption features. We generated the residual profiles by subtracting from each observation a broadened and veiled standard spectrum, using as standard stars the ones previously selected for the veiling calculations.

Although the residual method often enhances features such as weak emission lines (see Fig. 8, *top*), care must be taken during the subtraction, as a small difference in continuum normalization between the two spectra can also introduce false features. The uncertainty in the veiling determination and the difficulty of choosing suitable standard stars are other factors that can introduce errors in the process. Finally, the legitimacy of the concept itself is dubious when the overlying emitting region is optically thick over most of the profile.

The residual profile calculation suppresses, in principle, all the photospheric contribution that is present in the spectra, generating smoother profiles, as the broad lines are no longer superposed with narrow absorption ones. However, we noticed that it did not a priori enhance the redshifted absorptions present in our unsubtracted spectra; indeed, some of the redshifted absorption components turned out to be mainly photospheric (for example, the Na D lines of BP Tau, DF Tau, DQ Tau, and RY Tau; see Fig. 8, *bottom*). In general, most of the redshifted absorptions became shallower, although less noisy, and we did not find many new ones. Our residual profiles show that about 50% of our stars present at least one line with a redshifted absorption component, a result in agreement with the original (unsubtracted) data, with the magnetospheric models, and with the results by Muzerolle et al. (1998a), but not with Edwards et al. (1994). Although very weak features such as the iron emission lines and the redshifted absorptions at free-fall velocities are strongly affected by the underlying photospheric spectrum, one may notice that the general characteristics of the line profiles discussed in this work are weakly affected by the subtraction of the photospheric features and that our results are also valid for residual profiles.

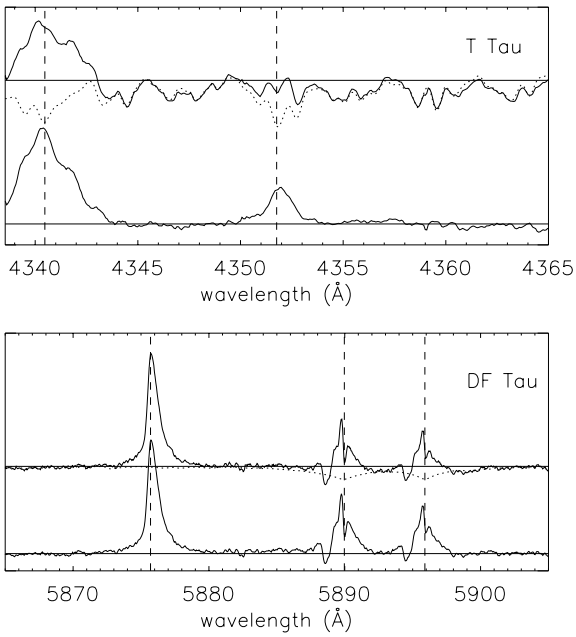

FIG. 8.—Residual profile determination. The upper solid lines correspond to the original spectra, the dotted lines to the standard spectra, and the lower solid lines to the residual CTTS profiles. *Top*: Fe II (λ4352) is dramatically enhanced by the residual method. *Bottom*: the redshifted absorption that appears in the unsubtracted spectrum in the Na D lines turns out to be mainly photospheric.

Finally, in agreement with both the model predictions and with Edwards et al. (1994), we see less evidence of redshifted absorption in Hα at high velocities than in the upper Balmer lines, probably because of thermalization effects and the Stark damping of the Hα wings.

4.5. *Profile Symmetry*

The magnetospheric accretion models predict that the BC emission is formed in the magnetospheric infalling material. It should then exhibit a central or slightly blueshifted peak and blueward asymmetry due to occultation by the disk and star of part of the flow moving slowly away from the observer. By blueward asymmetry we mean that there is an excess of blue emission compared to the red emission. Some theoretical profiles published by Hartmann et al. (1994) also show redshifted absorption at free-fall velocities, while others show extended red wings caused by the occultation of the high-velocity blueshifted material by the star; both effects add up to enhance the line asymmetry.

One way to search for asymmetries is to reflect one of the line wings about the broad emission centroid, as done by Johns-Krull & Basri (1997) for DF Tau. If the wings match each other, the line is considered symmetric, and this avoids a confusion between lines that are only shifted and lines that are really asymmetric. P Cygni profiles are more difficult to evaluate, since the blue emission wing is sometimes completely absent, and it may be hard to determine the correct shift to be applied.

In Table 4 we show the velocities that produced the best agreement between the opposite wings, and we also indicate which parts of the line are symmetric and which are not in the case of partially symmetric profiles. The BCs that showed blueward asymmetry are labelled "ASb" in Table 4, but they comprise only about 20% of the analyzed lines. Most of the BCs are symmetric (well fitted by a Gaussian) and about 75% of them have a central or slightly blueshifted peak. In Figure 9 we show the velocity position of the broad emission peak for several lines and we notice that, although most of them are indeed blueshifted, a substantial number present a redshifted peak. This is not seen in the published theoretical magnetosphere profiles. Lines with P Cygni profiles and those where the emission component was not reliably extracted are not included in this plot.

TABLE 4

WING SYMMETRY REFLECTION VELOCITIES (km s^{-1})

Star	Hα	Hβ	Hγ	Hδ	Ca II λ8662	Ca II λ8498
AA Tau.....	−30	ASb	ASb:	ASb	0[a]	−14[a]
AS 209.....	2	2	10	0	5	−7
AS 205.....	0[b]				−10	−10:
AS 353.....	0	20:	0:	0:	0	−10
BP Tau	ASb[b]	ASb[b]	ASb[b]	ASb	0	0
CI Tau.....	−10				0	−5
CO Ori	23	x	x	x	x	x
CW Tau	0	10	x	x	5	ASr[c]:
DE Tau.....	0	12	ASb[b]		7:	0
DF Tau.....	0	−18	−27	ASb:	ASb:	ASb:
DG Tau	−33	−33	20	20	5	ASr[d]
DK Tau	ASr[b]	ASb:	ASb	ASb	ASr:	ASr:
DL Tau.....	0	8	10	20	0	ASr[d]
DN Tau	AS*	ASb[c]	0	0	0[a]	−8[a]
DO Tau	0	−3	x	x	−6	−4
DQ Tau	ASr[d]	ASr[d]	−6	−10	ASb	ASb
DR Tau	0	0	−20	0	ASr[c]:	ASr[c]:
DS Tau	−35	−50	−30	−35	−9[a]	−12[a]
GG Tau	ASb[b]:	0	5	40	ASr	0
GK Tau	ASb[b]	−35	−25		−4[a]:	−5[a]
GM Aur.....	ASb[d]	−50:	−30	ASb	0[a]	−5[a]
GW Ori	0	−22	x	x	ASb[c]:	0
HL Tau.....	0				ASb[b]	−8
RW Aur	ASr[c]:	10	x	x	ASb[b]	ASb
RY Tau.....	ASr[d]	x	x	x	ASr	5
SU Aur	−13:	x	x	x	x	x
T Tau.....	0	−5	15:	0	−5	−10
UX Tau	−42				−8[a]	−15[a]
UY Aur.....	ASb[b]	−15	−20		ASb:	ASb:
V410 Tau....	ASb	x	x	x	x	x

NOTE.—Lines for which the cell is left blank were not available and as "x" were not reliably measured or observed in absorption. ASb means that the line is blueward asymmetric and ASr redward asymmetric.

[a] Only the narrow component is present.

[b] Only the high velocity is symmetric; the rest of the line is asymmetric.

[c] Only the low velocity part is symmetric; the wings at high velocities are asymmetric.

[d] The high and low velocities are asymmetric; the line part between those is symmetric.

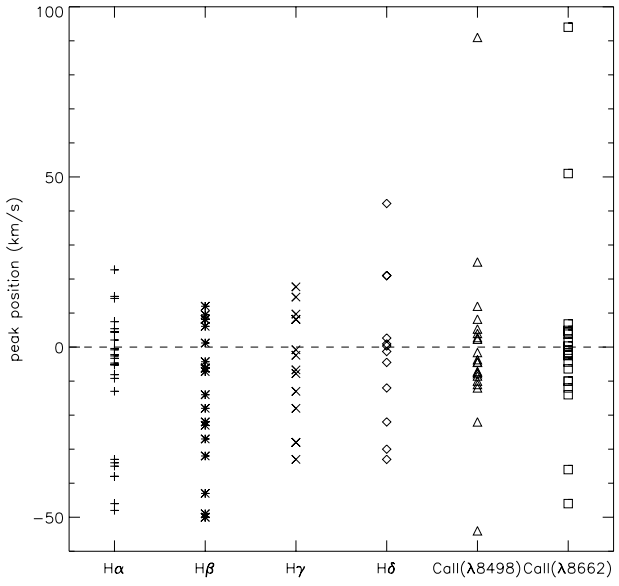

FIG. 9.—Broad emission component's peak position. Lines with P Cygni profiles and those not reliably measured are not included.

Among the lines that presented asymmetries, the ones identified as "ASb[c]" have symmetric low velocity material and a blueward excess of high-velocity emission, and those identified as "ASr" show redward asymmetries. Neither type is predicted by the magnetospheric model. Some lines do present profiles with the characteristics described by the magnetospheric models, corresponding to "ASb" and "ASb[b]" in Table 4. Examples of profiles in agreement and opposite to the magnetospheric symmetry predictions are shown in Figure 10 with the reflected wings overplotted.

Each Ca II IRT line is blended with a Paschen emission line, and this could lead to a wrong asymmetry classification. However, from the 13 stars that presented IRT asymmetries, only four could be due to the Paschen contribution, which affects the high-velocity wing redward of the line center. These stars are quoted as uncertain asymmetry measurements in Table 4.

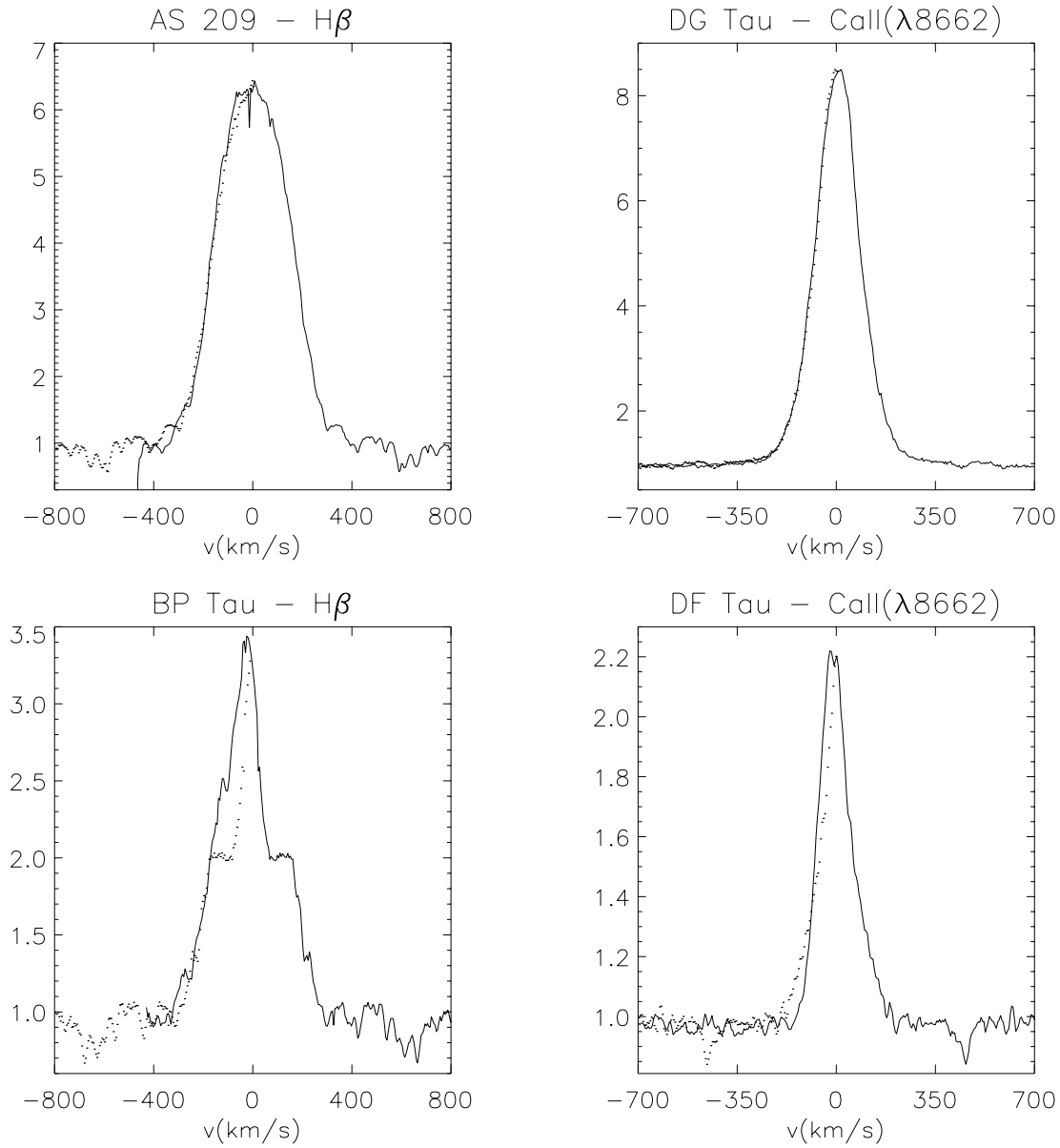

FIG. 10.—Emission lines with red wings (*dotted lines*) reflected. The top lines are symmetric and the bottom ones are asymmetric and in agreement with the magnetospheric model predictions.

In general, the symmetry predictions of the magnetospheric model cannot be strongly confirmed with our sample. Contrary to them, most of the BCs are found to be symmetric; among the asymmetric ones many are not blueward asymmetric, and about 20% of the broad emission components present centroids redshifted by more than 5 km s^{-1}.

5. DISCUSSION

Many aspects of the line formation of a CTTS can be inferred from the correlations found with the veiling-corrected equivalent widths in the previous sections.

We showed that lines coming from a common lower level are very well correlated, such as Hβ with Hα and the IRT lines with each other. This is expected, as they need the same physical conditions to be produced and tend to be affected by the same physical processes. As previous studies also showed, most lines have more than one component (BC and NC for the He I and the Ca II and emission and absorption components for the Balmer and Na D lines). These are likely formed in distinct regions, as the characteristics of those components are very different from each other throughout our sample and many correlations found were valid for one of the components but not for the other. According to our data, the Balmer emission, the He I BC, the IRT BC, and the iron lines (when in strong emission) are mainly formed in the magnetospheric flow. Alternatively, the He I BC may also come from the shock region, where the temperatures are high and more appropriate for the formation of that line instead of the magnetospheric flow itself. The NCs of the Ca and He I lines are thought to be formed at the stellar surface, where it is perturbed by the

infall of material and partly in the normal stellar chromosphere. The wind is the origin of the blueshifted absorption commonly seen in the Na D and Balmer lines.

We also verified that the effect of accretion on the line components sometimes probably produces the correlations, as lines formed in regions with physically distinct properties (very different temperatures, for example) but both affected by accretion can be found to correlate very well, such as the He I and the IRT NCs.

Somewhat puzzling is the lack of strong correlation between the IRT BCs and the Hα emission or the He I BCs, if all broad emission lines are supposed to share a common forming region. Johns-Krull & Basri (1997), analyzing DF Tau, confirm the lack of correlation found between the IRT BC and the Hα emission, but they found a correlation between the He I BC and the IRT that neither we nor Muzerolle et al. (1998a) confirm in our samples of various CTTSs.

We showed that the IRT lines and Hα are good mass-accretion indicators in our sample. We also confirmed that the same mechanism that powers the accretion also seems to influence the outflow, as the emission and absorption components of Hα are well correlated with the mass-accretion rates and with each other. Other good evidence for the accretion-wind connection is that the Fe lines in strong emission seem to be related to both processes, occurring when the wind and the veiling are prominent.

The blueshifted absorption components are thought to be formed in low-density winds. There is strong evidence that the NCs are formed at the stellar surface (Batalha et al. 1996). Although they are both influenced by the accretion process, they should not be compared to the theoretical magnetospheric profiles.

Some of the observations tend to support the fact that the accretion affects the relatively quiet stellar atmosphere, and lines produced in that region suffer the influence of such changes. The models also predict that accretion and outflow should be related to each other—the former occurring through closed magnetic field lines that connect the disk to the star and the latter through the open field lines escaping from the disk itself.

However, the results presented in the previous sections also show that some of the general characteristics of the magnetospheric accretion models are not always confirmed by our data. The idea that the broad emission components mainly arise from a common emitting region, the infalling magnetospheric gas according to those models (Hartmann et al. 1994), must be taken with care, as the observational evidence is not yet conclusive. We must also keep in mind that the magnetospheric predictions do not do particularly well for the broad emission components to which they primarily apply. We find observed profiles to be generally fairly symmetric, with centroids distributed through a range of blueshifted to redshifted velocities. Sometimes they have redshifted absorption components, but often not at free-fall velocities. Only about 20% of the BC profiles support the specific predictions of the models.

Hartmann et al. (1994), Muzerolle et al. (1998b), and Muzerolle et al. (1998a) presented line profiles generated with magnetospheric models and compared them with observational ones. They obtained good agreement between the observed and theoretical profiles of many lines for some stars, such as BP Tau. But, comparing their BP Tau observed profiles with ours, many differences can be seen. This is expected, as CTTSs are known to exhibit line profile variability sometimes even within a few hours (Johns & Basri 1995a), and Gullbring et al. (1996) showed that this is the case for BP Tau, a typical CTTS. The problem that arises with the rapid profile variation is that, even if the magnetospheric models can reproduce one of the profile types of a star, it does not mean that all the profiles that a line may exhibit will be reproduced without changing basic model characteristics. As an example, the model used to compare the observed and theoretical profiles of BP Tau cited above does not fit our observations of that star well.

Some years ago, Shu et al. (1994) proposed a new version of their X-celerator mechanism whose natural period was the rotational period of the star. Lines formed in magnetospheric accretion flows that are controlled by the stellar field might also show periodicity at the stellar rotation period in the presence of an inclined dipole field. In this case, the line variations would certainly be due to geometrical effects, and a model with the same basic parameters should be able to describe the various line profiles. SU Aur presented this kind of variations in Hβ and Hα (Johns & Basri 1995b), but unfortunately its profiles do not resemble the published theoretical ones very much.

In general, however, the line variations do not seem to be related to orbital motion as they do not usually correlate with the stellar rotational period. Different parts of a line may vary differently, as Johns & Basri (1995a) showed by analyzing time variations of Hα for several CTTSs. They suggest the line-emission region is composed of discrete, stochastically varying blobs with a range of velocities and turbulence, which the Sobolev treatment used in the actual magnetospheric models does not take into account.

Najita et al. (1996), analyzing Brγ emission profiles, showed that WL 16, an obscured low-luminosity YSO, presented profiles that were remarkably similar to the theoretical Balmer line calculations by Hartmann et al. (1994). Later, Muzerolle et al. (1998b) calculated profiles for the Brγ emission and showed that, in fact, the WL 16 Brγ emission line was very well reproduced. However, some of the stars in the sample of Najita et al. (1996) also present very symmetric emission profiles, such as AS 353, DG Tau, and SVS 13, that cannot be explained only by magnetospheric accretion. Although the magnetospheric model can generically explain part of the large line widths and the occasional redshifted line absorptions, it does not predict symmetric profiles, because the magnetospheric infalling material is subjected to occultation effects by the star-disk system.

Most of our broad emission profiles were found to be symmetric and the few asymmetries occur on both the blue and the red side. Due to these differences, the profiles presented in the theoretical papers generally do not match our observed ones. Many authors have speculated on the origin of the rather symmetric broad line wings in TTS profiles. Basri (1990) suggested that the wings were formed in a turbulent region near the star, and Edwards et al. (1994) pointed out that Alfvén waves could generate the necessary turbulent broadening. Johns & Basri (1995b) managed to reproduce some of the Balmer line symmetric features of SU Aur by adding a range of turbulent high-velocity components at the base of spherically symmetric wind models, and Johns & Basri (1995a) could also fit the DF Tau wings with a similar procedure.

Most of the stars discussed here rotate slowly ($v \sim 10$ km s^{-1}) at velocities that are much smaller than the velocities of

the infalling material ($v \sim 200$–300 km s^{-1}) and the inclusion of rotation in the theoretical models will not significantly alter the profiles in this case. Even in the case of a stiff magnetosphere, material coming from a disk at $3R_\star$ would have $v \sim 30$ km s^{-1} and would not influence the entire line. The addition of winds to the theoretical models will certainly change the line shapes, but stars such as AS 209 and DE Tau, which do not always exhibit blueshifted absorption and are rather slow rotators, will still need some further explanation of their broad symmetric line profiles (Fig. 1).

Stark broadening may explain the low very broad far wings in Hα (Hartmann et al. 1994 and Muzerolle et al. 1998b), but it will not produce the main Gaussian shape commonly present in many different lines. A better treatment of the radiative transfer (actually done with the Sobolev method) could also alter the theoretical line profiles and would properly take into account Stark and opacity broadening effects.

Magnetospheric accretion probably does occur in CTTS. Evidence for it includes hot spots at the stellar surface of these stars, thought to be due to the magnetic accretion shock, redshifted absorption components at free-fall velocities that would be hard to explain without magnetospheric infall, as well as cases like SU Aur and WL 16 that give more explicit support to the theory. However, it may not be the only important mechanism. The symmetry of the line profiles and the lack of correlation of the variation among different line regions suggest an important turbulent process may be occurring together with the magnetospheric infall.

6. CONCLUSIONS

We have presented the spectral analysis of a sample of CTTSs covering a wide range of optical wavelengths and veilings. We tested the predictions of the magnetospheric accretion model and previously published results supporting them. We confirm that many CTTSs exhibit central or blueshifted broad emission lines but a substantial minority show redshifted centroids. The accretion and outflow seem to be related and redshifted absorption components are sometimes present in the spectra. We found that the analysis and interpretation of these is not straightforward. We could not reproduce the observational results that showed a very high frequency of redshifted absorption in the lines of CTTSs. We also show that most of our emission components are symmetric, instead of blueward asymmetric as predicted by the theory or suggested by previous observational studies. We saw that the broad components of different atomic lines are not strongly correlated to each other, while we would expect them to be if they were all formed in the accretion flow.

Our results do not refute the general magnetospheric accretion scenario, but rather indicate that it is only part of the important processes that produce the strong permitted line emission in CTTSs. Our intent is to point out that the case has not yet been strongly made, and that much more observational and theoretical work is required. Part of the emission-line profiles may also be produced in winds, and rotation and turbulence must be added to the models.

Synoptic observations are critical to understanding the full range of profiles produced by a single star, where some underlying parameters do not change but others do, and many structures are dynamic.

This research is based on data collected on the Shane 3 m telescope at Lick Observatory run by the University of California. We would like to thank Christopher Johns-Krull, Anthony Misch, Michael Bisset, Claude Bertout, Natalie Stout-Batalha, and Celso Batalha who helped gather the profiles presented here. S. H. P. A. acknowledges support from the Conselho Nacional de Desenvolvimento Científico e Tecnológico, Brazil.

REFERENCES

Appenzeller, I., Reitermann, A., & Stahl, O. 1988, PASP, 100, 815
Basri, G. 1990, Mem. Soc. Astron. Italiana, 61, 707
Basri, G., & Batalha, C. C. 1990, ApJ, 363, 654
Basri, G., & Bertout, C. 1989, ApJ, 341, 340
Basri, G., Johns-Krull, C. M., Mathieu, R. D. 1997, AJ, 114, 781
Batalha, C. C., Stout-Batalha, N. M., Basri, G., & Terra, M. A. O. 1996, ApJS, 103, 211
Beristain, G., Edwards, & S., Kwan, J. 1998, ApJ, 499, 828
Bertout, C., Basri, G., & Bouvier, J. 1988, ApJ, 330, 350
Calvet, N., Basri, G., Imhoff, C. L., & Giampapa, M. S. 1985, ApJ, 293, 575
Calvet, N., Basri, G., & Kuhi, L. V. 1984, ApJ, 277, 725
Choi, P. I., & Herbst, W. 1996, AJ, 111, 283
Edwards, S., Hartigan, P., Ghandour, L., Andrulis, C. 1994, AJ, 108, 1056
Edwards, S., et al. 1993, AJ, 106, 372
Gullbring, E., Petrov, P. P., Ilyin, I., Tuominen, I., Gahm, G. F., & Lodén, K. 1996, A&A, 314, 835
Hamann, F., & Persson, S. E. 1992, ApJS, 82, 247
Hartigan, P., Edwards, S., & Ghandour, L. 1995, ApJ, 452, 736
Hartmann, L. 1998, Accretion Processes in Star Formation (Cambridge: Cambridge Univ. Press)
Hartmann, L., Calvet, N., Avrett, E., & Loesler, R. 1990, ApJ, 349, 168
Hartmann, L., Calvet, N., Gullbring, E., & D'Alessio, P. 1998, ApJ, 495, 385
Hartmann, L., Edwards, S., & Avrett, E. 1982, ApJ, 261, 279
Hartmann, L., Hewett, R., & Calvet, N. 1994, ApJ, 426, 669
Herbig, G. H., & Bell, K. R. 1988, Lick Obs. Bull., 1111, 1
Herbst, W., Rhode, K., Hillenbrand, L. A. 1999, AAS Meeting, 194, 68.03
Johns, C. M., & Basri, G. 1995a, AJ, 109, 2800
———. 1995b, ApJ, 449, 341
Johns-Krull, C. M., & Basri, G. 1997, ApJ, 474, 433
Mundt, R., & Eislöffel, J. 1998, AJ, 116, 860
Muzerolle J., Calvet N., & Hartmann L. 1998b, ApJ, 492, 743
Muzerolle J., Hartmann L., & Calvet N. 1998a, AJ, 116, 455
Najita, J., Carr, J., & Tokunaga, A. T. 1996, ApJ, 456, 292
Natta, A., & Giovanardi, C. 1990, ApJ, 356, 646
Shu, F., Najita, J., Ostriker, E., Wilkin, F., Ruden, S., & Lizano, S. 1994, ApJ, 429, 781
Stassun, K. G., Mathieu, R. D., Mazeh, T., & Vrba, F. J. 1999, AJ, 117, 2941
Valenti, J. A. 1994, Ph.D. thesis, Univ. California, Berkeley
Vogt, S. S. 1987, PASP, 99, 1214